ChemComm

Homogeneous Catalysis of Dioxygen Reduction by Molecular Mn Complexes

Journal:	*ChemComm*
Manuscript ID	CC-FEA-08-2022-004628.R1
Article Type:	Feature Article

Homogeneous Catalysis of Dioxygen Reduction by Molecular Mn Complexes

Emma N. Cook and Charles W. Machan*

* - machan@virginia.edu; ORCID 0000-0002-5182-1138

E.N.C. ORCID: 0000-0002-0568-3600

Department of Chemistry, University of Virginia, PO Box 400319,

Charlottesville, VA 22904-4319

Abstract

Continually increasing global energy demand perpetuates the need for effective alternative energy sources and 'green' industrial processes. The oxygen reduction reaction (ORR) is crucial to the development of hydrogen fuel cells, a key device in the development of alternative energy sources. Further, the ORR to hydrogen peroxide by electrochemical means can provide an environmentally friendly alternative to its industrial production, which is capital and energy intensive. While Pt has traditionally been the best electrocatalyst for the ORR, inspiration from active sites in nature that bind and transport O_2 has led to the development of earth-abundant transition metal catalysts. However, despite the prevalence of Mn-based active sites that bind and activate O_2 there remains a lack of developed Mn-centered catalysts for ORR in comparison to Fe and Co. Here, we summarize known Mn-based electrocatalysts for the ORR and describe their activity as well as future directions of the field.

1. Introduction

The utilization of dioxygen (O_2) in synthetic and catalytic processes has long been inspired by its life-sustaining roles in nature, where it is essential for energy utilization, the degradation of harmful substances, metabolism, and the synthesis of important biomolecules.[1-5] Due to its natural abundance, researchers have been working to utilize the oxidative power of O_2 as an alternative oxidant in capital and energy intensive processes. Industrial production of commodity chemicals, complex organic molecules and fuels from petrochemical feedstock relies on selective C–H bond activation and oxidation, where current processes often require the use of a stoichiometric oxidant and have poor selectivity.[6] Selective electrochemical utilization of O_2 in these processes would provide an affordable and abundant alternative with low toxicity (**Figure 1**).

The oxygen reduction reaction (ORR) is also of interest for alternative energy and fuel cell applications (**Figure 1**). Polymer electrolyte membrane fuel cells are the most promising alternative for automotive power generation, with the advantage of high energy output and low emission profile.[7] These fuel cells function through the oxidation of molecular hydrogen into protons and electrons, coupled with the proton-dependent reduction of O_2 to water (H_2O). The alternative ORR product, hydrogen peroxide (H_2O_2) is used in a wide range of industrial processes including paper bleaching, wastewater treatment, and as a 'green' oxidant in chemical industry.[8, 9] The current industrial anthraquinone process for the production of H_2O_2 is capital intensive and uses fossil fuel-derived H_2. Further, H_2O_2-based fuel cells are becoming increasingly attractive as an alternative energy device.[10] With the increasing global energy demand, depletion of non-renewable fuel sources, and the environmental impact of current capital-intensive industrial processes, affordable and 'green' alternatives are crucial moving forward, however, expensive and platinum-based catalysts are commonly used for mediating the ORR and new fundamental understanding is required to develop replacements.

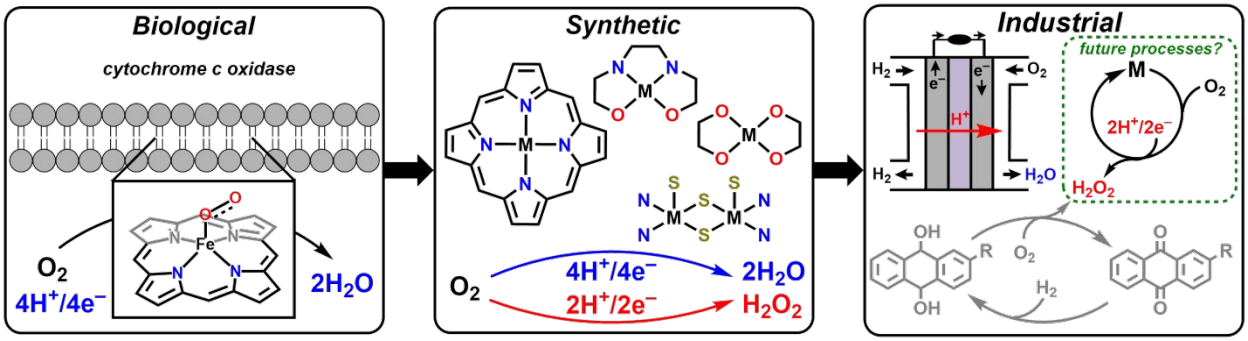

Figure 1. Summary of relevant O_2 reduction in biological, synthetic and industrial chemistry. M = transition metal.

One challenge in the activation and reduction of O_2 is its triplet ground state, which inhibits reactivity with singlet organic substrates with limited spin polarization.[11] Nature has overcome this by employing open-shell transition metal centers that favorably react with O_2. Iron, copper, and manganese (Mn) are most commonly found in enzymatic active sites that activate O_2 due to their redox flexibility and their natural abundance. Some notable examples of these include hemoglobin, dioxygenases, lipoxygenases, monooxygenases, and superoxide dismutase, among many others.[1, 2, 12-18] Mn is also

found in the only enzyme active site which oxidizes water during photosynthesis (the oxygen evolution reaction, OER), which is the reverse reaction of the $4H^+/4e^-$ ORR. The Oxygen Evolving Complex (OEC) in Photosystem II contains a Mn_4CaO_5 cluster and the Mn atoms are thought to be the key active sites for O–O bond formation.[19, 20] The OEC has inspired an expanding field of Mn-based electrocatalysts for the OER.[21-23] These bioinorganic systems have inspired the development of a variety of synthetic compounds for O_2 activation.[24] The prevalence of earth-abundant first-row transition metals for O_2 reduction in nature has led to of the development of homogeneous ORR catalysts based on manganese, iron, cobalt, and copper active sites.[4, 25] However, despite the prevalence of Mn-centered enzymatic active sites for O_2 activation and reduction,[24] there remains a lack of synthetic Mn-based electrocatalysts for the ORR in comparison to iron and cobalt.

Our group has been motivated by the sparse number of Mn-based electrocatalysts for the ORR and has focused on developing porphyrinic and non-porphyrinic Mn-centered catalysts that reduce O_2. Here, we describe advancements in the development of Mn-centered electrocatalysts for the homogeneous ORR and provide our perspective on the current state and future of the field. We will also provide analysis on the controlling factors of the ORR at Mn active sites, in comparison to Fe- and Co-based catalysts, emphasizing important differences and the potential advantages of Mn as an active site.

For the purposes of this perspective, we are excluding Cu-based systems[26], heterogeneous systems based on molecular Mn active sites, and single atom Mn catalysts, but we direct interested readers to a number of relevant reviews and articles on heterogeneous and immobilized Mn-based catalysts for the ORR.[27-43]

2. Catalytic O_2 Reduction Mediated by Mn

As introduced above, relative to later first-row transition metal centers, there are fewer examples of homogeneous catalyst systems based on Mn. It is challenging to assess an exact first example, given that O_2 consumption in aerobic reactions can be of secondary importance to the oxidative conversion of interest. One of the first examples of catalytic ORR by a molecular Mn system was disclosed by Hamilton and Revesz in 1966 (**Figure 2**).[44] Interest in developing models to understand the function of amine oxidases led to studies on an amine oxidase mimic based on catalytic amounts of pyridoxal and Mn. Amine oxidases use dioxygen to convert alkylamines into aldehydes with ammonia as a

co-product, producing hydrogen peroxide as the result of simultaneous ORR.[45] Hamilton and Revesz found that under slightly basic conditions (pH 9.1), alanine could be catalytically decomposed to pyruvate and ammonia. Reaction stoichiometry implied that H_2O_2 was produced as a co-product from O_2, although it was not observed during the reaction. However, control testing showed that H_2O_2 is rapidly consumed under reaction conditions, consistent with previous reports on the aqueous chemistry of Mn(III) ions with H_2O_2.[46] It was proposed that pyridoxal and the alanine substrate undergo a condensation reaction under catalytic conditions to form a transient imine-containing active species with the Mn ion. It is this Schiff base-type species (**Figure 2**), which was proposed to bind O_2 and facilitate the oxidation reaction.

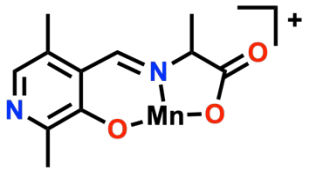

Hamilton and Revesz, 1966

Figure 2. Catalytically relevant intermediate in amine oxidation activity, the condensation product of pyridoxal and glycine in the presence of Mn(III).[44]

Following this report, Bettelheim *et al.* reported the electrochemical properties of Mn(III) 5,10,15,20-tetrakis-(4-*N*,*N*′,*N*″-trimethylanilinium)porphyrin pentachloride (**Figure 3A**) under aqueous conditions, including in the electrocatalytic reduction of dioxygen, in 1983.[47] In phosphate buffer with added NaCl (pH = 8), adsorption was observed (equilibration time <5 min), and the electrode was determined to have monolayer coverage of the Mn-based porphyrin complex. Analysis of the voltammetric response with respect to scan rate under catalytic conditions was used to propose that H_2O_2 was the major product. The authors did not describe whether a significant difference in activity was observed when comparing solutions of the Mn-based porphyrin complex with electrodes covered by a molecular monolayer; mentioning only that a positive shift in the catalyst standard potential was observed, consistent with favorable O_2 binding following the Mn(III)/(II) reduction. Subsequently in 1985, Nagao *et al.* conducted a study on electrocatalytic ORR mediated by Mn(III) 5,10,15,20-tetrakis-(1-methylpyridinium-4-yl)porphyrin pentachloride under aqueous conditions (**Figure 3B**).[48] Although variable

scan rate data suggested a homogeneous response under inert atmosphere, exposure to solutions with >1 mM concentrations of the porphyrin was found to result in adsorption and the voltammetric response was noted to be similar for the modified electrode in a blank solution and the prepared Mn porphyrin solutions at concentrations of 57-65 micromolar. However, the stability of the adsorbed Mn porphyrin was found to be limited during ORR, where H_2O_2 was the major product, suggesting incompatibility between adsorbed catalyst and reaction product. Based on rotating ring-disk voltammetry (RRDV), a second-order rate constant of 1.1 x 10^6 $M^{-1}s^{-1}$ was determined for the ORR to H_2O_2. Analogous adsorption phenomena for the analogous Fe-based porphyrin have been described more recently.[49]

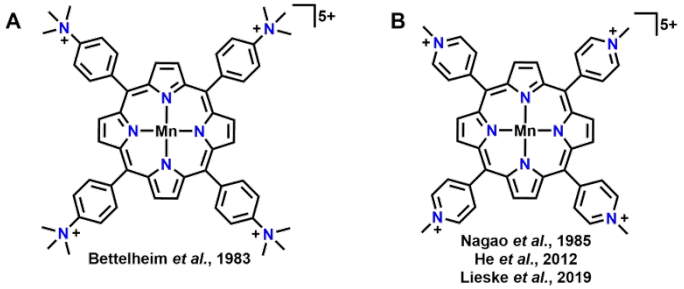

Figure 3. Structures of charged Mn(porphyrin) derivatives examined for ORR under aqueous conditions: (**A**) Mn(III) 5,10,15,20-tetrakis-(4-*N*,*N*′,*N*″-trimethylanilinium)-porphyrin and (**B**) Mn(III) 5,10,15,20-tetrakis-(1-methylpyridinium-4-yl)porphyrin.[47]

Concurrent with the report by Nagao *et al.*,[48] Evans and Sheriff disclosed the production of H_2O_2 during ORR in a pH range of 7.5-8.6 by combining Mn(II) with (4,5-dihydroxybenzene-1,3-disulfonate) as a catalyst (**Figure 4**).[50] Solutions of hydroxylamine provided the electrons and protons necessary to drive the reaction with turnover numbers observed in excess of 10^4. A follow-up study in 1992 by Sheriff showed that substituted catechol moieties were also active toward ORR, although none of these combinations demonstrated better activity than the original sulfonated derivativederivates.[51] Hydrazine was also determined to be a suitable reductant when substituted for hydroxylamine. Notably, activity with Co, Cu, or Fe ions substituted for Mn produced significantly lower activity. It was proposed that a bis(catecholate) Mn complex was the active species under reaction conditions and that the O atoms coordinated to Mn played a key role in

supporting the binding of the monodeprotonated hydroxylamine reductant through a hydrogen bonding interaction, prior to an electron transfer to O_2.

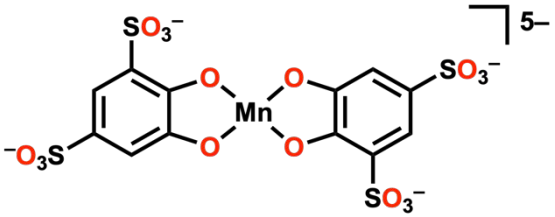

Evans and Sheriff, 1985

Figure 4. Mn(III) bis(catecholate) complex proposed as the active species for the most active catalytic system reported by Evans and Sheriff.[50]

In 1989, Fukuzumi and co-workers reported a pair of studies on the use of ferrocene derivatives as chemical reductants in the ORR mediated by metallotetraphenylporphyrins.[52, 53] In both studies, Mn (**Figure 5**) was compared to Co and Fe in MeCN solution with perchloric acid as the proton donor. The reaction product was not directly characterized for Mn; the Co-based analogue was proposed to generate water via a 2+2 mechanism where the production of H_2O_2 was mediated by Co and H_2O_2 was reduced by the presence of excess ferrocene derivatives. Despite having a standard reduction potential 0.5 V more negative than Co, the Mn derivative had a lower catalytic second order rate constant of 1.4 x 10^5 $M^{-1}s^{-1}$, compared to 1.1 x 10^6 $M^{-1}s^{-1}$ for Co under the same conditions when decamethylferrocene was used as the reductant. Unlike ferrocene, the decamethylferrocene derivative has a reduction potential which is more negative than both catalyst standard potentials.[54]

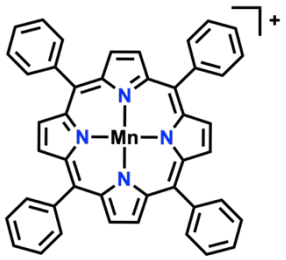

Fukuzumi and co-workers, 1989

Figure 5. Mn(III) 5,10,15,20-tetrakisphenylporphyrin reported as an ORR catalyst by Fukuzumi and co-workers in 1989.[52, 53]

The next example of catalytic dioxygen reduction by a homogeneous Mn complex was a non-porphyrinic system reported by Borovik and co-workers in 2011.[55] The supporting ligand framework, bis[(N′-tert-butylurealy)-N-ethyl]-(6-pivalamido-2-pyridylmethyl)-aminato, contains two N-coordinated monodeprotonated urea moieties and a carboxyamido group which is O-coordinated to Mn(II) for steric reasons as part of an overall $[N_4O]^{3-}$ primary coordination sphere ($[Mn(H_2bupa)]^-$; **Figure 6**). Exposure to dioxygen rapidly produced an intermediate end-on Mn(III) peroxo species in the presence of diphenylhydrazine (or hydrazine), with net proton and electron transfer occurring to the N atom of the O-coordinated carboxyamido group and O_2, respectively. Over the course of five hours, the Mn(III) peroxo species converted to a terminal Mn(III)–O species stabilized by significant proton donation from the carboxyamide arm, resulting in structural character that is intermediate between oxo and hydroxo end states. This intermediate Mn(III) oxo/hydroxo could be converted back to the starting Mn(II) state with water release in the presence of diphenylhydrazine (overall two electron/two proton reduction reaction). Since the formation of the Mn(III) oxo/hydroxo intermediate also required an overall two electron/two proton reduction with water release, this system became catalytic when an excess of diphenylhydrazine and O_2 were present in solution. Turnover numbers as high as 200 could be observed, with the elevated concentrations of the water product degrading the catalyst beyond this point. The authors proposed that a key mechanistic aspect was the participation of two different types of hydrogen bond donors with different pK_as and steric geometries, which could stabilize intermediates and participate in formal transfers with different parameters. The development of biologically inspired secondary coordination spheres which participate in the reaction has become increasingly important in the development of active and selective molecular catalysts for a variety of redox-based transformations.[56-65]

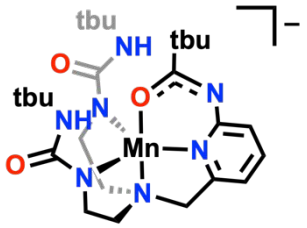

Borovik and co-workers, 2011

Figure 6. Mn-based $[Mn(H_2bupa)]^-$ catalyst with secondary-sphere moieties capable of hydrogen bonding with and proton transfer to O_2 and ROSs reported by Borovik and co-workers.[55]

He *et al.* also studied the electrocatalytic performance of Mn(III) 5,10,15,20-tetrakis-(1-methylpyridinium-4-yl)porphyrin pentachloride in aqueous conditions (**Figure 3B**), using 0.1 M aqueous solutions of trifluoromethanesulfonic acid as the supporting electrolyte.[66] Although not directly measured, trifluoromethanesulfonic acid is expected to fully dissociate and generate a working solution with a pH = 1.[67] Under these conditions, the Mn porphyrin produced H_2O_2 as the primary product, with a comparable second order rate constant (10^4 $M^{-1}s^{-1}$) to the Co analogue which produced the same majority product, in spite of the standard potential for Mn which was measured to be 0.2 V more reducing under reaction conditions. Adsorption of the complex was not observed and catalyst degradation was not described, although Bettelheim *et al.* had observed instability below pH < 3.6 for the related Mn(III) 5,10,15,20-tetrakis-(4-*N*,*N*′,*N*″-trimethylanilinium)porphyrin pentachloride complex **(Figure 3a)**.[47] In our own report on Mn(III) 5,10,15,20-tetrakis-(1-methylpyridinium-4-yl)porphyrin pentachloride, we noted an instability at pH ≤ 3 in the Mn(II) state during spectroelectrochemical experiments using Britton-Robinson Buffer, *vide infra*.[68]

Abu-Omar, Fukuzumi and co-workers disclosed in 2015 that Mn(III) corroles could catalyze the two-electron reduction of O_2 using octamethylferrocene as a sacrificial electron source and trifluoroacetic acid as the proton donor (**Figure 7**).[69] Unlike the known examples with porphyrins, this system is proposed to have a Mn(III) active state which can react with O_2 to produce a Mn(IV) superoxide intermediate. Mechanistic studies showed that the reaction rate had a first-order dependence on the concentrations of the catalyst and O_2 (and was independent of the concentrations of trifluoroacetic acid and octamethylferrocene), which the authors ascribed to a catalytic cycle with O_2 binding and reduction by one-electron as the rate-determining step. Product analysis suggested that H_2O_2 was the nearly exclusive product. Unlike the previous studies by Fukuzumi and co-workers,[52] no reduction of the H_2O_2 product by octamethylferrocene was observed, which can likely be attributed to the use of the relatively weaker trifluoroacetic acid as a proton

donor instead of perchloric acid. Although a Mn(V) arylimido was the catalyst precursor, the following reduction and protonation to release a primary arylamine in the catalytic reaction only required Mn(IV)/(III) cycling for ORR to occur.

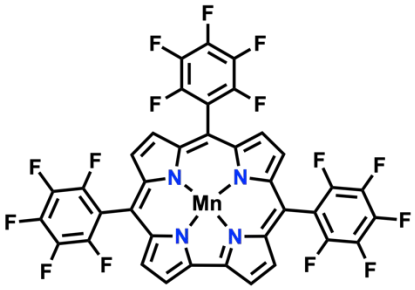

Abu-Omar, Fukuzumi and co-workers, 2015

Figure 7. The resting state of the catalytic cycle proposed by Abu-Omar, Fukuzumi and co-workers: Mn(III) 5,10,15-tris(pentafluorophenyl)corrole.[69]

Duboc and co-workers then published a unique example of a dinuclear Mn catalyst based on a dithiolate-modified 2,2′-bipyridine ligand (**Figure 8**).[70] When the dipotassium salt of the ligand was exposed to a stoichiometric amount of manganese, a dinuclear Mn complex with a single thiol ligand was isolated (*N.B.* both Mn centers retained the divalent oxidation state of the precursor perchlorate salt). We note that the stoichiometric chemistry of Mn complexes with thiolate containing ligands and O_2 has been explored extensively by Kovacs and co-workers.[71-75] Upon exposure to dry air, both centers were oxidized by a single electron and a bridging hydroxide species was recovered. Mechanistic studies established that the dinuclear monothiol species united two separate reaction cycles, where either H_2O_2 or H_2O production was favored. The isolated μ_2-hydroxo species is situated on a stoichiometric reaction cycle, which produces water in the presence of sufficient acid. Although the dinuclear monothiol Mn(II) complex can be regenerated electrochemically, only 35% of the material is recovered following electrolysis. Conversely, octamethyl- and decamethylferrocene can be used to establish a catalytic cycle for ORR in the presence of 2,6-lutidinium tetrafluoroborate as an acid with H_2O_2 as the primary reaction product. The authors ascribed the product differentiation as a consequence of the relative concentrations of acid to the dinuclear Mn complex under catalytic and stoichiometric conditions: high acid concentrations favor protonation of the M–O bond while at low concentrations O–O bond scission can occur.

Interestingly, the Fe-based analogue of this Mn system was later shown to have a product dependence based on whether an electrode or soluble chemical reductant was used: under electrochemical conditions the electrode was capable of reducing key intermediates and favoring O–O bond cleavage to produce water, while the diffusion-limited process of reduction by dissolved ferrocene derivatives instead favored H_2O_2 release through M–O bond protonation.[76]

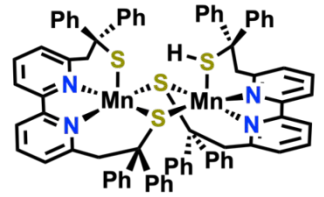

Figure 8. Dinuclear catalyst developed by Duboc and co-workers based on a dithiolate-modified 2,2′-bipyridine ligand.[70]

Noting the relatively limited examples of electrochemical ORR mediated by Mn complexes, we became interested in identifying strictly homogeneous electrocatalysts (adsorption equilibria with the electrode surface were not observed or implied). We noted that a feature of many general synthetic preparations for Mn complexes is to begin with a Mn(II) precursor and ligand under aerobic conditions and isolate a Mn(III) complex.[77] Curious about the generality of this observation for salen- and salophen-type ligand frameworks,[78] we were interested in related ligand frameworks which did not contain potentially reactive imine bonds.[79] Based on prior studies conducted by Arora et al.,[80] we developed an alternative Pd-catalyzed method for isolating the 6,6′-di(3,5-di-*tert*-butyl-2-hydroxybenzene)-2,2′-bipyridine (^{tbu}dhbpy(H)$_2$) ligand in high-yield.[81] Exposure to a suitable base and Mn(II) precursor under aerobic conditions allowed us to isolate the Mn(III) complex Mn(^{tbu}dhbpy)Cl (**Figure 9**).[81] In MeCN solvent with 2,2,2-trifluoroethanol present as a weak acid, this compound was found to be ca. 80% selective for H_2O_2 production during the electrocatalytic ORR using RRDV methods.

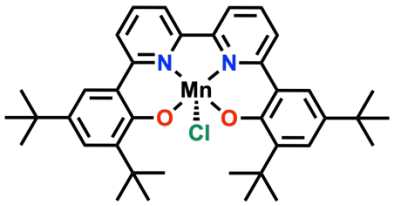

Machan and co-workers, 2018

Figure 9. Mn(^{tbu}dhbpy)Cl catalyst developed in our group.[81]

Under electrochemical conditions, our mechanistic testing revealed a catalytic reaction mediated by Mn(^{tbu}dhbpy)Cl which showed first-order dependence on the concentrations of catalyst, O_2, and proton donor. Further, the Mn(III)/(II) reduction couple showed a sensitivity to the concentration of the added proton donor that was independent of a Cl^- ion loss equilibria. This was ascribed to a protonation continuum involving the Mn-bound O atoms of the ligand in the Mn(II) state, as established through the use of a potential-pK_a diagram.[82] Control testing suggested that the less-than-quantitative production of H_2O_2 was the result of a Mn-mediated disproportionation reaction. On the basis of these data, we proposed a catalytic cycle where the reduction and protonation of a Mn(III) superoxide intermediate was the rate-limiting step in the reaction, k_3 in **Figure 10**.[83]

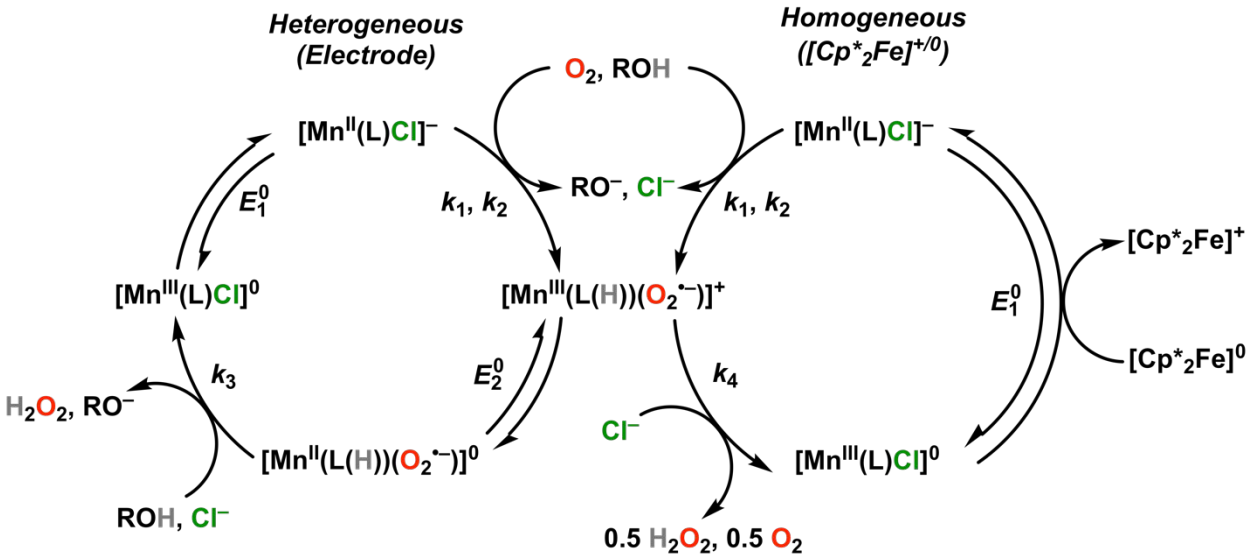

Figure 10. Electrocatalytic and electrochemical catalytic cycles for Mn(^{tbu}dhbpy)Cl; L(H) indicates monoprotonation of the phenolate groups of the ligand framework.[83] Reprinted with permission from *J. Am. Chem. Soc.* **2019**, *141*, 4379–4387. Copyright 2019 American Chemical Society.

Subsequently, we became interested in using thermodynamic reaction control[4, 84] to decrease the overpotential for H_2O_2 formation.[83] At overpotentials (η) as low as 20 mV, electrocatalytic turnover frequencies of 7.82 s^{-1} were observed. The η of an electrocatalyst for the ORR is defined as the difference in the applied potential (E_{appl}) and the equilibrium potential of the reaction (E_{ORR}) under experimental conditions.[4] Under electrochemical conditions with buffered proton donors (equivalent amounts of proton donor and its conjugate base) a strong dependence on acid pK_a was observed and no catalytic activity occurred when the system was placed under counterthermodynamic conditions with respect to the standard potential of H_2O_2 production (catalyst standard reduction potential was positive of the reaction standard potential). However, replacing the electrode with decamethylferrocene as a source of electron equivalents resulted in identical rates for the electrochemical ORR using same set of buffers with Mn(^{tbu}dhbpy)Cl, implying a mechanistic change had occurred. Under chemical reduction conditions, we proposed that the Mn(III) superoxide intermediate proposed from electrochemical studies is a branching point between two overlapping catalytic cycles. At low proton donor activity and concentration, the catalytic wave contains two distinct features, which we assigned to the Mn(III)/(II) reduction that triggers O_2 binding, and the proton-dependent reduction of the resultant Mn(III) superoxide. In other words, the second electron transfer requires more reducing conditions. Since the reducing power of the decamethylferrocene chemical reductant is fixed, the driving force for the second electron transfer decreases, allowing a disproportionation reaction to occur whereby H_2O_2 and O_2 are generated in equal amounts.

Following our initial report on Mn(^{tbu}dhbpy)Cl,[81] Nocera and co-workers reported a study on the electrocatalytic behavior of manganese porphyrins in MeCN solvent, comparing the effects of including a pendent proton donor in the secondary coordination sphere (**Figure 11**).[85] For Mn(III) 5,10,15,20-tetrakis-phenylporphyrin chloride, H_2O was observed as the majority product across a range of pK_as and the rate law showed a first-order dependence on [Mn] and [O_2], with a second-order dependence on [acid], leading the authors to propose that hydrogen bond-assisted stabilization of a Mn(III) superoxide intermediate was important, prior to further reduction. The rate-limiting step was proposed

to be a proton transfer-assisted O–O bond cleavage to generate a Mn(V) oxo intermediate which is rapidly reduced and protonated to release water under experimental conditions. Consistent with this, the use of the pendent proton donor changed the rate dependence on [acid]: at low concentrations of added acid, the system showed a first-order dependence, reflecting the participation of the pendent proton donor in stabilizing the peroxide intermediate (**Figure 11**). A shallow Brønsted slope was obtained in the comparison of proton donor pK_a with the catalytic rate constant, which was ascribed to the role of the two equivalents of acid in driving an electron transfer that is not rate determining to generate the pre-catalytic Mn(III) peroxide state. It was also noted that the use of strong acids promoted demetallation at sufficient concentrations under experimental conditions in MeCN, which was determined by the appearance of a new redox wave that matched the response of the free base porphyrin ligand.

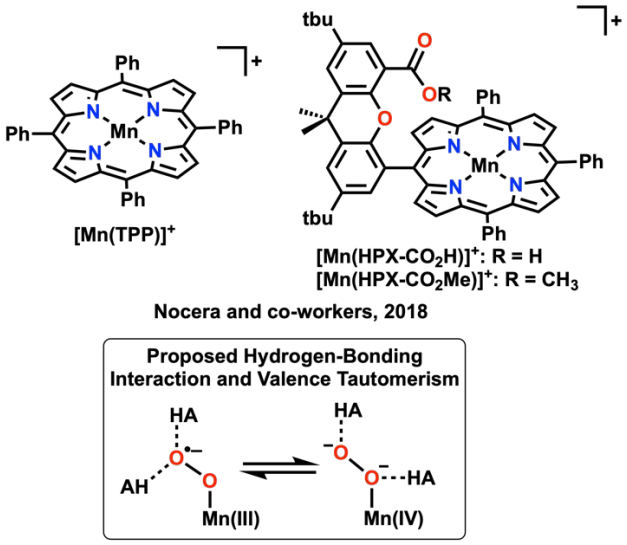

Figure 11. Mn(porphyrin)-based catalysts examined by Nocera and co-workers. Non-covalent interactions with hydrogen bond donors were proposed to impact the equilibrium resonance structure of the Mn-O_2 adduct. The inclusion of pendent proton sources in the hangman ligand framework was reflected in changes in the observed rate law at low acid concentrations; HA indicates added Brøntsed acid or pendent proton donor.[85]

Motivated by these precedents, we re-examined the reported behavior[48, 66] of Mn(III) 5,10,15,20-tetrakis-(1-methylpyridinium-4-yl)porphyrin pentachloride under aqueous conditions (**Figure 3B**).[68] Contrary to these previous reports, which showed selectivity for

H_2O_2 using phosphate buffer (pH = 7) and 0.1 M trifluoromethanesulfonic acid (pH = 1) in indirect product analyses based on rotating disc electrochemistry (RDE), we found selectivity ranging between 82-93% for H_2O across a pH range of 3-6 with pH-adjusted Britton-Robinson buffer. Measurements at lower pH were precluded by the demetallation of the Mn complex, as had been reported previously under strongly acidic conditions,[47, 85-87] and at higher pH because of a significant background ORR response by the electrode. Control experiments showed that the selectivity for H_2O is not likely to be the result of a 2+2 mechanism in the pH range of 3-6, as expected from previous reports.[88, 89] Using potential-pH analysis and UV-vis spectroelectrochemistry, we proposed that the active Mn(II) species was five-coordinate, with an axial water ligand opposite the site of O_2 binding.[90-92]

More recently, we returned to our Mn(^{tbu}dhbpy)Cl catalyst to develop a method to shift selectivity from H_2O_2 to H_2O (**Figure 12**).[93] Anson and Stahl had demonstrated that the combination of Co(salophen) and *p*-hydroquinone resulted in a co-electrocatalytic system for the ORR.[94] Based on prior mechanistic studies,[95] they showed that electrogeneration of *p*-hydroquinone occurs under conditions where Co(salophen) binds and activates O_2 through a single electron transfer. The resultant Co(III) superoxide is rapidly reduced by sequential HAT and proton-coupled electron transfer reactions from the electrogenerated *p*-hydroquinone, resulting in a product selectivity shift from H_2O_2 (without *p*-hydroquinone) to H_2O (with *p*-hydroquinone). Given that our Mn-based complex is also proposed to have an important intermediate peroxide,[81, 83] we reasoned that redox mediators which transfer proton and electron equivalents to the catalytically active site could also be used to enhance its activity and shift product selectivity. In contrast to the work of Anson and Stahl, we elected to use a much weaker acid that should only monoprotonate the electrogenerated *p*-benzoquinone dianion under the conditions of the reaction.[96-105] The non-ideal solvent mixture of MeCN with molar concentrations of 2,2,2-trifluoroethanol resulted in the favorable solvation of the dianion by 5-6 equivalents of the proton donor (K_{eq} = 2.31 x 10^6 with 2.5 mM *p*-benzoquinone and 1.37 M 2,2,2-trifluoroethanol).[93] In this non-ideal solvation environment, two proton transfers became thermodynamically feasible, although trifluoroethoxide base is assumed to remain strongly associated in solution and oxidation of the reduced quinone core was expected to favor proton transfer

back to 2,2,2-trifluoroethanol.[97, 106, 107] Interestingly, the non-covalent assembly of weak proton donors with the reduced quinone was found to be more reactive than *p*-hydroquinone,[94] however, it did not have intrinsic ORR activity and similarly shifted product selectivity from H_2O_2 to H_2O (96%) while increasing the observed activity (**Figure 12**). Based on our studies, we proposed that the observation of a product selectivity change could be attributed to the reduced and hydrogen bond-stabilized quinone mediator transferring one proton and two electrons to the Mn(III) superoxide intermediate as part of a new co-catalytic mechanism.

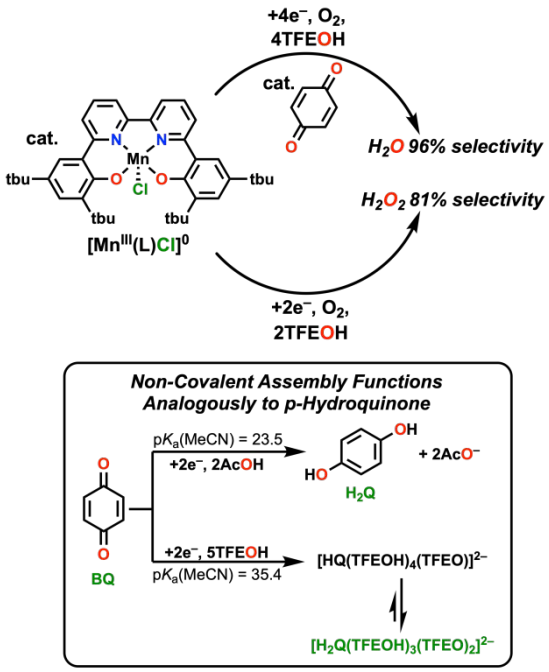

Figure 12. A product selectivity switch from H_2O_2 to H_2O is observed upon the inclusion of a *p*-benzoquinone (BQ) as a redox mediator in the presence of excess weak acid, TFEOH.[93] Adapted with permission from *Chem. Sci.* **2021**, *12*, 9733–9741. Copyright 2021 Royal Society of Chemistry.

3. O_2 Activation and Reduction

The molecular orbital description of O_2 gives essential context about its ground state and reactivity. Dioxygen exists in a triplet ground state where the highest occupied molecular orbitals are singly occupied degenerate π^* orbitals, giving the molecule an overall bond order of 2. A single reduction of O_2 to a superoxo ($O_2^{\bullet-}$) reduces the bond order to 1.5, with a formal $2e^-$ reduction to a peroxo (O_2^{2-}) species cleaving the O–O π-

bond entirely.[108] Oxidation reactions involving O_2 are often thermodynamically favorable, however, there is often a significant kinetic barrier due in part to its triplet ground state which makes reactivity with closed shell substrates a spin-forbidden process, under the assumption that the substrate experiences a minimum of spin polarization in its ground state.[11]

Conversely, O_2 activation by open-shell transition metals can be highly favorable (**Figure 13**). O_2 activation at a metal center results in the formation of reduced O_2 intermediates, known as reactive oxygen species (ROS), whose stability is crucial in determining reaction pathways. The binding mode of O_2 to a single metal center is dependent both on *d*-electron count and spin configuration of the metal, as well as the steric properties invoked by the supporting ligand framework. O_2 can bind in an end-on (**13A**) or side-on fashion (to either one **13B** or two metal centers **13D**) and this interaction typically results in formal oxidation of the metal center and reduction of O_2 to generate metal superoxo ($O_2^{\bullet-}$) or peroxo (O_2^{2-}) species. In addition to the σ-symmetric interactions possible with the lone pairs on each O atom, the π bond can also act as a σ donor. The propensity to reduction upon binding is in part due to another aspect of the frontier orbital structure of O_2, specifically, the partially occupied degenerate π^*-symmetric SOMOs. Upon coordination with a metal center, these energetically accessible orbitals can act as a π-acid and accept electron density through a π-backbonding interaction, lowering bonding character.

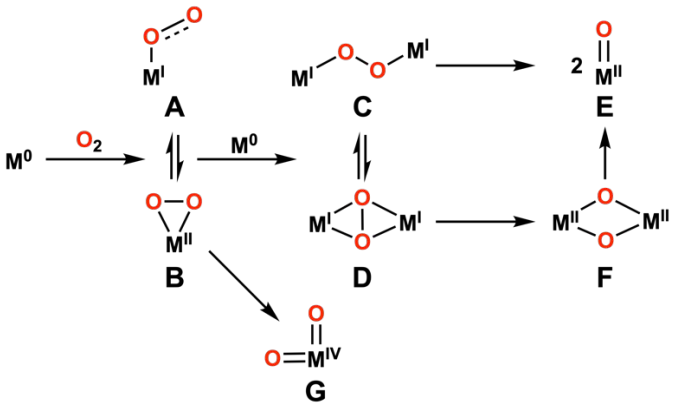

Figure 13. Summary of possible reaction pathways for aprotic O_2 activation in mono- and dinuclear configurations.

Generally, the end-on binding mode of metal superoxide is bent (**13A)** rather than linear. This is because the *σ* bond with the metal center arises from a fully occupied *π** orbital (generated through the formal one electron reduction of O_2) acting as a Lewis base and donating electron density into the d_{z^2} acceptor orbital of the metal. Depending on the oxidation state of the metal, an additional *π*-interaction from partially filled d_π metal orbitals into the remaining singly occupied *π** orbital of O_2 is possible; strong coupling between these orbitals is responsible for the diamagnetic structure of Fe(III)-superoxides in porphyrinic frameworks.[25, 109] In a side-on binding mode, the σ bond originates from a *σ*-symmetric interaction involving donation from the *π*-orbital of O_2 into the d_{z^2} orbital of the metal, with π-backbonding from the metal's filled d_π orbitals into the partially occupied π* orbitals of O_2. O_2 can also act as a bridging ligand between two metal centers in a μ-η^1:η^1 **13C** or μ,η^2:η^2 fashion **13D** with each metal providing an electron to achieve an overall two-electron reduction to an O_2^{2-} configuration. Ligand structure can be used to modulate the character of the frontier *d* orbitals, as well as inhibit specific binding modes through control of the stereochemical profile.[4, 110, 111]

Catalytic Reduction of O_2

During the electrocatalytic reduction of O_2, product selectivity is controlled, in part, by the nature of O_2 binding to the active site, which dictates the extent of ROS stabilization and the nature of the reactivity for intermediates formed through the mechanistic cycle. In a protic media, there are two primary pathways for the ORR a $2H^+/2e^-$ transformation to make H_2O_2 or a $4H^+/4e^-$ process to form two equivalents of H_2O. Generally, ORR to both H_2O_2 and H_2O mediated by *mononuclear* catalysts is initiated by electron transfer from a metal active site to O_2 to form a metal-bound $O_2^{\bullet-}$ as described above (**Figure 14**, ***iii***).[4, 8, 112] From here, a proton and electron transfer can occur in either a stepwise or concerted fashion to form a hydroperoxo intermediate (OOH^-), (**Figure 14**, ***iv***). Formation of H_2O_2 arises from favorable net reduction of the complex and protonation of the proximal oxygen based on the adsorption strength of the OOH^- species to the metal center and its consequences for the basicity of the M–O bond. The mechanistic pathway to H_2O formation commonly arises from protonation of the M–OOH adduct at the distal O atom, assisted by electron transfer from the metal center, leading to cleavage of the O–O bond,

release of one equivalent of H_2O and the formation of a high valent metal oxo (O^{2-}) species (**Figure 14**, ***v***). Subsequent transfer of $2e^-$ to the metal and $2H^+$ to O^{2-} releases the second equivalent of H_2O. ORR to generate H_2O can also proceed via a 2+2 mechanism, where H_2O_2 produced during catalysis can be further reduced to two equivalents of water by the catalyst. There are a number of factors that govern mechanistic pathways and favorable formation and stability of reactive intermediates. For catalysts which form dinuclear species on the catalytic cycle, superoxide formation is generally avoided in favor of peroxo intermediates which can undergo aprotic or proton assisted cleavage to generate μ-oxo or -hydroxo species prior to further reduction and protonation to release H_2O.

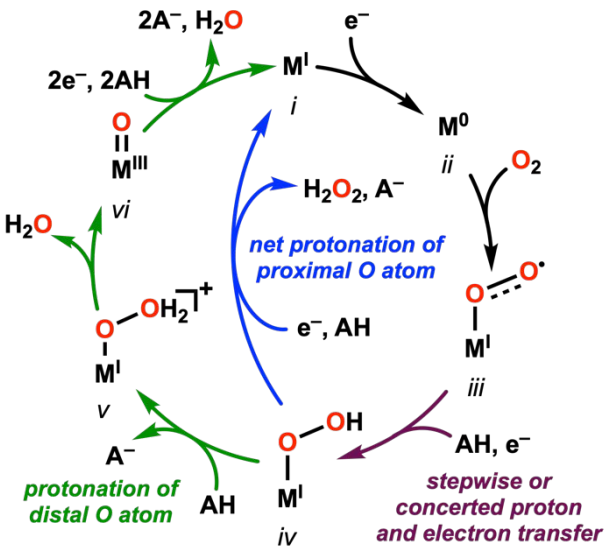

Figure 14. Generalized mechanism for the ORR at mononuclear active sites.

In fuel cells, the ORR to H_2O is preferred due to its higher free energy release as well as it being non-destructive to these devices. The standard redox potential of O_2 reduction to H_2O is +1.229 V vs. SHE. By comparison the $2e^-/2H^+$ reduction of O_2 to H_2O_2 is less thermodynamically favorable, with a more negative standard reduction potential of +0.68 V vs SHE.[112] However, further reduction of H_2O_2 by $2e^-/2H^+$ to two equivalents of water is very favorable, with a standard reduction potential of +1.77 V vs SHE.[112] When comparing electrocatalysts, overpotential (η) and turnover frequency (TOF) are common metrics that assess efficiency and activity. As described above, η describes the thermodynamic comparison of catalyst operating potential with the minimum reduction

potential required under operating conditions.[4] TOF is given in reaction rate per unit time, reflecting how rapidly product is generated under catalytic conditions. An effective catalyst minimizes overpotential while maximizing TOF. The essential challenge to developing better electrocatalysts for O_2 reduction (and indeed any catalyst) is how to prevent the release of reactive intermediates during catalysis to prevent side reactions and catalyst deactivation. Moduli of control in the testing and regulation of the possible reaction pathways include the redox potential of the catalyst, the electronic and steric effects imparted by the primary and secondary coordination spheres.

Analysis of Dioxygen Adduct Structure in Mn/Co/Fe

Clearly, there is a large disparity in the available information on Mn-centered systems relative to Fe and Co-based ones. However, comparing Mn to Fe and Co is informative to the development of better catalysts. First, we must consider the ability of different metal centers to bind O_2 based on frontier orbital configuration and reduction potential.[113] Based on the limiting approximation of the Sabatier Principle, for ORR to occur the catalytic metal center must not bind any intermediate species, such as $O_2^{\bullet-}$, OOH, and OH, too weakly or too strongly.[114] It is worth emphasizing that many different scaling relationships are possible with molecular systems, but that within catalyst families intrinsic parameters like reduction potential can scale proportionately with activity because of a relatively uniform relationship to the stability of intermediates and/or the energy of the rate-determining transition state.[115, 116]

A 2014 study by Flyagina *et al.* used single-hybrid DFT functional methods to examine the primary differences in the ORR catalyzed by Mn, Fe and Co in four different macrocyclic ligand frameworks.[117] They found that while O_2 binding was dependent on the nature of the metal center and the macrocycle structure, binding to Mn was the strongest in all frameworks, with the side-on configuration preferred. The binding interaction between Co and O_2 was found to be the weakest and only occurred in an end-on fashion. The behavior of Fe was intermediate to these two extremes, binding O_2 in both end-on and side-on configurations. Next, the complete catalytic cycles were assessed for model systems of the ligand frameworks with each metal center by including an OH^- group *trans* to the site of O_2 binding. Given the relatively lower catalytic response

predicted for Mn in this class of active site in comparison to Fe and Co, the authors proposed that its O_2 binding strength impedes the kinetics of subsequent reaction steps. The Fe macrocycle was predicted to be the most active of the three and catalyzes the ORR via a concerted $4e^-/4H^+$ pathway. In comparison, although both pathways were feasible, Mn was able to catalyze the $2e^-/2H^+$ pathway faster than the $4e^-/4H^+$ due to the unfavorable second protonation of the distal O atom during catalysis.[117] Further, in comparison to Fe and Co, the protonation of the intermediate bis(hydroxide) species during the $4e^-/4H^+$ pathway to generate an equivalent of water bound to the metal center was significantly less favorable for Mn, indicative of greater thermodynamic stability. Qualitatively speaking, this has been observed experimentally by Fukuzumi and co-workers, who found that Mn-based catalysts were the slowest of the three under otherwise identical reaction conditions.[52, 53]

A parallel study by Baran *et al.* disclosed a computational analysis on electrochemical ORR mediated by porphyrinic first row transition metal complexes which included an assessment of the role of secondary coordination sphere interactions on catalysis using a gradient-corrected DFT functional.[118] This study found that the binding energy of metal-bound –OH, –O, and –OOH intermediates decreased moving from left to right on the periodic table, meaning again that Mn binds these intermediates more strongly than Fe and Co. Interestingly, the difference between the M–OH and M–OOH binding energies remains constant across the first row transition metals, suggestive of an intrinsic scaling relationship between these intermediates. A comparison of the base metal macrocycle with a comparable 'hangman' scaffold containing a carboxylic acid provided adequate conformational flexibility to stabilize the M–O intermediate through a hydrogen bonding interaction (see **Figure 11** for an example of a 'hangman' ligand). The study found that substituting sulfonic acid for the carboxylic further stabilized the M–O intermediate, which was attributed to its decreased pK_a.[118] Overall, they found that the higher activity of the hangman metalloporphyrins relative to the unfunctionalized porphyrin arises from a combination of the destabilization of M–OH and M–OOH intermediates due to the inclusion of electron-withdrawing groups at the *meso* positions of the porphyrin in addition to the stabilization of M–O intermediates by the hangman carboxylic acid group.[118]

Explaining why Mn binds O_2 and its reduced intermediates more strongly than Fe and Co is not trivial, but there are several important factors to consider. It is generally accepted that the Fe(II) in porphyrinic frameworks binds O_2 in an end-on fashion after reducing it by one electron and that the primary bonding interactions arise from an interaction between the vacant d_z^2 of the low-spin Fe(III) center and the fully occupied π^* orbital of $O_2^{\bullet-}$, antiferromagnetically coupled as ^{2}Fe(III)-$^2O_2^{\bullet-}$, **Figure 15**.[119] In comparison, Mn has been shown to prefer to bind O_2 in a side-on configuration in porphyrinic frameworks and prefers to be in a high-spin state.[110, 120] In this geometry, calculations performed using second-order perturbation theory indicate that the major resonance contributor is the ^{4}Mn(IV)-$^1O_2^{2-}$ resonance form (minor ^{3}Mn(III)-$^2O_2^{-}$), where two electrons have been formally donated from the Mn center to O_2 (**Figure 15**).[121] The obvious difference is that the Fe center prefers a low-spin configuration upon O_2 binding and a single electron transfer while the Mn center prefers a high-spin one, with a final electronic state which is a resonance-averaged electron transfer greater than one but less than two. Mn(II) has a high spin-pairing energy relative to later first row transition metals and strong ligand fields are required to achieve low-spin configurations in octahedral environments.[111] Low-spin states become slightly more accessible for Mn(III), which is also prone to Jahn-Teller distortion, but the preference is still for a high-spin configuration. Consistent with the trend for the divalent and trivalent formal oxidation states, the d^3 configuration of Mn(IV) prefers an open-shell configuration.

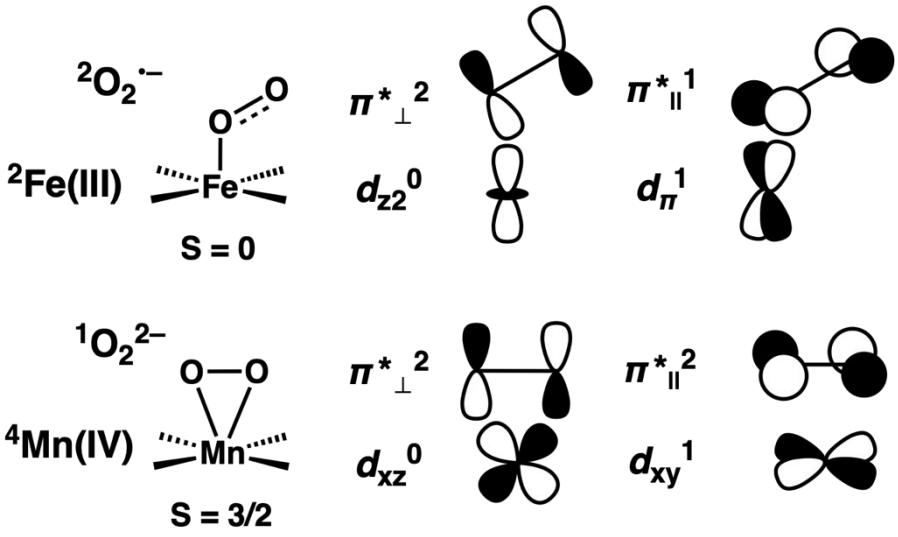

Figure 15. Comparison of the electronic structures proposed for O_2 adducts formed upon exposure to Mn(II) and Fe(II) porphyrins.

Phung and Pierloot have proposed that O_2 binding to Mn(II) in the porphyrinic framework occurs through sequential electron transfer events.[121] The relatively slow step is the initial electron transfer from Mn(II) center occurring between its singly occupied d_{xz} orbital and the π^* orbital perpendicular to the metal-dioxygen bonding axis, forming a π-symmetric bonding interaction. The resultant adduct is in a formally quartet spin manifold, which crosses into a different quartet spin manifold as the distance between Mn and O_2 shortens during bond formation. At the minimum energy crossing point between these two different quartet spin manifolds, a second electron transfers from Mn d_{x2-y2} into the π^* orbital parallel to the M-O_2 bond axis. The resultant fully occupied π^* orbital is δ symmetric with respect to the Mn d_{xy} orbital (**Figure 15**), resulting in a weak interaction which primarily resembles the parallel π^* orbital on O_2^{2-}. This means that the singly occupied d_{xy} orbital is formally antibonding with respect to this δ-symmetric interaction and the singly occupied d_{yz} and d_{z2} orbitals form negligible interactions with O_2^{2-}. It is reasonable to speculate that the relative inflexibility of the Mn spin manifold which manifests in this preference for side-on binding is also a contributor to the observed ORR activity and selectivity. Relative to an end-on superoxide adduct with distal and proximal O sites, a side-on peroxide adduct will have symmetric O atoms that are relatively less basic thanks to interactions with the high-valent Mn center. For formal cleavage of the O–O bonding interaction to occur in the mononuclear side-on peroxide adduct, adjacent oxo/hydroxo species need to form (**Figure 13G**), which isn't sterically accessible within a rigid macrocyclic ligand framework. In the event that the formation of a bridging dinuclear Mn peroxide adduct is sterically accessible, the O atoms are again likely to be less basic and formal O–O bond cleavage would result in the possibility of strong electronic coupling between the unpaired spin of the Mn centers in the resultant Mn_2O_2 core (**Figure 13D** and **F**).[74, 122]

Critical Analysis of Homogeneous ORR by Molecular Mn/Fe/Co

Extensive studies on ORRs mediated by metalloporphyrins allows for a critical comparison of activity and mechanism for structurally analogous systems containing Fe, Co and Mn active sites. Generally, Co catalysts have shown a preferred selectivity for H_2O_2 under homogeneous conditions, unlike Fe-based porphyrins that exclusively make H_2O. This has been attributed to the fact that the formation of an intermediate high-valent metal-oxo species is less thermodynamically accessible for octahedral Co complexes than Fe.[69] However, as described above, computational studies indicate the thermodynamic feasibility of both reaction pathways for Co. Inspired by these and examples of selectivity for H_2O for ORR mediated by surface-immobilized molecular species, Stahl and co-workers used Brønsted acid scaling relationships to switch reaction selectivity by thermodynamically excluding certain reaction pathways in DMF. When both reaction products are thermodynamically feasible, the kinetic product H_2O_2 is preferred; when H_2O_2 generation is no longer thermodynamically viable, the system switches to H_2O production.[123] Co(II) porphyrins are known to readily react with dioxygen, forming end-on superoxide adducts with a low-spin Co center, ^{1}Co(III)-$^2O_2^-$.[109, 124-126] Proton-coupled electron transfer (either stepwise or concerted), produces a Co(III)-OOH intermediate which is the selectivity branching point between the two catalytic pathways. With a sufficiently weak acid, the protonation of the M–O bond of this hydroperoxo intermediate becomes endergonic. Instead, reduction and protonation of the distal O atom of the Co-bound hydroperoxide transfer occurs to cleave the O–O bond and generate a putative Co(III) oxyl species with concomitant water formation *en route* to further reduction and protonation to generate a second equivalent of water. The mechanism of homogeneous ORR mediated by Fe(TPP) (TPP = tetraphenylporphyrin) in DMF and MeCN has been described in extensive detail by Mayer and co-workers.[116, 127, 128] They determined that a pre-equilibrium for reversible O_2 binding to Fe(II) leads to the formation of an end-on Fe(III)-superoxide species, which has been described in detail above. The protonation of the distal O atom of this end-on superoxide species is the rate-determining step of the reaction: subsequent reduction and protonation by $3H^+/3e^-$ is comparatively rapid and closes the catalytic cycle and produce two equivalents of water. Subsequent mechanistic studies investigations with Fe(5,10,15,20-tetrakis-(mesityl)porphyrin) chloride showed that the production of H_2O_2 from an Fe(III)-OOH intermediate requires the dissociation of

the hydroperoxide anion and does not show a rate dependence on the concentration of added acid, unlike the proton-dependent behavior observed for comparable Co systems.[129]

We can contrast these observations to the results with Mn-based porphyrins in MeCN, reported by the Nocera group.[85] The observed second-order dependence of activity on acid concentration for Mn, is in direct contrast to the analogous Fe and Co systems discussed above: Fe and Co exhibit a first-order dependence on acid during H_2O production. For comparison, Co shows a first-order dependence on acid during H_2O_2 production while Fe shows a zero-order dependence; Mn has not yet been shown to have activity for this product under comparable conditions. It was proposed that the second-order activity dependence on ORR to H_2O was a result of the stabilization of presumptive end-on Mn-based (su)peroxy intermediates through hydrogen bonding.[85] This suggests that an essential role of the added acid is to destabilize side-on (su)peroxide coordination in favor of the end-on mode and make the ORR to H_2O kinetically viable. Comparison with a carboxylic acid-modified 'hangman' derivative reinforces this description, reflected in stoichiometry changes of the rate law at low proton donor concentrations. Theory predicts that both the H_2O_2 and H_2O products are thermodynamically accessible for Mn,[117, 118] as was the case with Co, which implicates the possibility of analogous reaction selectivity control to that reported by Stahl and co-workers for the Co congener through Brønsted acid scaling relationships should also be possible with Mn. It is compelling that the side-on binding mode of (su)peroxide to Mn can be readily disrupted by non-covalent interactions since the alternative strategy accessing low-spin Mn to disrupt the kinetic limitations of this binding mode is potentially synthetically prohibitive. The results suggest that if the thermodynamic and kinetic trap of end-on coordination can be avoided through reaction or synthetic control, Mn centered catalysts can show significant ORR activity.

It is also possible to compare the ORR activity of salen-, salophen-, and acen-based (imine backbones) Co complexes reported by the Stahl group to the Co and Mn catalysts with a 2,2′-bipyridine (bpy) backbone developed by our group.[59, 81, 83, 130] Stahl and coworkers showed that the imine-based N_2O_2 derivatives of Co are selective for H_2O_2 in MeOH with acetic acid as a proton donor.[131] The observed turnover frequencies have a shallow dependence on the Co(III/II) reduction potential than the Fe-based porphyrins,

which is attributed to the influence of this redox event on only one kinetically relevant step (protonation), in contrast to two for Fe(porphyrin) derivatives (O_2 binding and protonation).[131] The experimentally determined rate law for Co imine-based N_2O_2 mediated ORR shows first-order concentration dependences on Co and acid, indicating that the resting state of the catalyst is a Co(III)-OOH species, the protonation of which is rate limiting (**Figure 14, blue**).[132]

We have also studied the bpy-based ligand framework discussed above for Mn with Co-centered catalysts.[59, 130] In contrast to what has been previously observed, this non-porphyrinic Co catalyst produces H_2O as the majority product during catalytic ORR. Despite a change in selectivity, the rate law of ORR by the $[Co(^{tbu}dhbpy)]^+$ catalyst is the same as Stahl's catalysts, with first order rate dependences on [Co] and [acid]. However, the observed product selectivity for water suggests the rate-determining step has shifted to protonation of the distal oxygen of a Co(III)-OOH species (**Figure 14, green**). We hypothesized that the increased *π*-acidity of the bpy backbone stabilizes the Co(III)-OOH intermediate by accommodating stronger *π*-donation from O to Co. In follow-up studies, the introduction of a pendent relay in the secondary coordination sphere of the bpy-based catalysts resulted in a shift of product selectivity and H_2O_2 becoming the primary product through a kinetic enhancement.[59] In other words, the effect of the pendent relay was to kinetically favor an analogous mechanism to the imine-based $Co(N_2O_2)$ complexes examined by Stahl and co-workers.

In comparison, the Mn analogue, $Mn(^{tbu}dhbpy)Cl$, mediates ORR with first-order catalytic rate dependence on [Mn], [acid], and $[O_2]$ concentration, similar to Fe(porphyrin) derivatives, but instead produces H_2O_2 as the primary reaction product like the imine-based $Co(N_2O_2)$ complexes. We have proposed that the reduction and protonation of an intermediate Mn(III) superoxide is rate-determining (**Figure 14, purple**) and have speculated that proton (or proton donor) acceptor ability of the inner-sphere phenolate moiety is important for the observed activity. In preliminary DFT calculations with a single hybrid functional,[83] both end-on and side-on modes were found to be thermodynamically accessible for Mn(III)-superoxide in this bpy-based ligand framework, suggesting that a blending of wavefunctions could exist similar to the Mn(porphyrin) system[85, 121, 133] and should be considered in the future with higher-level computational methods. In the context

of the discussion here, it can be hypothesized that the observed interactions of added proton donors and proton transfer to the Mn-bound phenolate moieties impact both steric and electronic parameters, shifting the distribution between side-on and end-on coordination modes during the catalytic cycle. Mechanistic work to assess how such considerations impact selectivity between H_2O_2 and H_2O through synthetic ligand iteration is ongoing.

Anson and Stahl have shown that an alternative to ligand modification strategies to achieve shifts in product selectivity is to design co-electrocatalytic systems.[94] Their report on the inclusion of co-catalytic amounts of benzoquinone to intercept an intermediate Co(III)-superoxide species via sequential HAT and subsequent PCET steps and shift product selectivity from H_2O_2 to H_2O, is an important example of how mechanistic understanding allows for the development of new catalyst systems. Our own work showed that this approach has generality to Mn catalysts with superoxide intermediates and that formal O–H bond formation is not necessarily a requirement. Taken together, it can be reasoned that if a fundamental challenge for Mn-based molecular catalysts is escaping the (su)peroxide state, redox mediators (which do not intrinsically show significant activity or selectivity during the ORR) are an excellent way to achieve emergent properties from Mn complexes. As a design principle, quantifying the O–H bond dissociation free energies (BDFEs) of Mn superoxide and hydroxide species can aid in selecting the appropriate redox mediator, but this must be reconciled to place the mediator reduction potential positive or equal to the catalyst standard potential. Indeed, knowledge of relative BDFEs has already been shown to be efficacious for designing co-electrocatalytic systems for alcohol oxidation and CO_2 reduction.[134-137]

The dinuclear Mn thiolate complex that catalytically reduced O_2 to H_2O_2 reported by Duboc and co-workers suggests an alternative strategy for Mn-based catalyst development.[70] Following the initial report, an Fe analogue of this catalyst for the ORR was disclosed.[76] For both Fe and Mn, it was found that the electron-rich thiolate ligand framework facilitated stabilization of metal-peroxo intermediates, decreased the activation barrier for O_2 binding, increased the reducing power of the metal center, increased the basicity of bound substrates, and intrinsically labilized *trans* ligand sites to support unsaturated coordination environments.[70] Additionally, catalytic studies

suggested that protonation of one of the thiolates to form a pendent thiol proton relay during O_2 activation is also important, protonating metal-peroxo intermediates to form a hydroperoxo species, ultimately leading to the cleavage of metal-O bonds and release of H_2O_2.[70, 76] The combination of intrinsic ligand properties, the redox reservoir enabled by a dinuclear active site, as well as the non-covalent and proton donor capabilities of a pendent relay contributed to avoid the potential thermodynamic sink of Mn_2O_2 species, thus, enabling catalysis.

Outlook and Conclusion:

The apparent lessons for Mn catalyst design that can be drawn from the analysis of these examples are summarized below:

- The propensity for high-spin configurations increases the bonding strength between Mn and O_2 (as well as ROSs), kinetically limiting turnover by favoring a thermodynamically stable side-on binding state. Non-covalent effects like hydrogen-bonding have been established as an effective method for favoring the end-on coordination mode and facilitating catalysis. Additionally, the use of a redox mediator can also enable reductive transformation of Mn-superoxide intermediates by generating molecules with low effective BDFEs.
    - Ligand frameworks which favor low-spin configurations are another possibility, although examples of these are limited and low-spin configurations have not been proposed for known Mn-based ORR catalysts. Further, in a low spin configuration in an octahedral environment, Mn(III) can still have more unpaired electrons than the comparable Fe(III) species. Since this spin is likely to be distributed in *π*-symmetric *d* orbitals, increased bonding strength with (su)peroxide species is still a possible limitation if strong coupling occurs with partially and fully occupied π* orbitals on the O_2^{n-} framework.
    - Ligand frameworks for mononuclear catalysts that either inhibit the formation of the side-on coordination mode of O_2 entirely or contain *cis* vacant sites are also possible opportunities. The former would avoid the

thermodynamic trap of the Mn(IV)-O_2^{2-} resonance state while the latter could make O–O bond scission from this state kinetically accessible.

- Multinuclear species offer a complementary opportunity to destabilize MnO_2 intermediates. The only known example relies on the unique donor properties of a highly charged thiolate-rich ligand framework, exemplifying how an understanding of structure-activity relationships from extensive stoichiometric mechanistic studies can be translated into competent catalytic systems.[24] Strong magnetic coupling between the unpaired spin on Mn centers through oxo/hydroxo bridges were avoided by these electronic effects combined with the participation of a pendent proton relay.
    - Dinuclear complexes with rigid ligand frameworks have not yet been disclosed, but these would enable precise control over interatomic distances. Examples abound in the design of molecular catalysts for water oxidation to dioxygen, which is the reverse of the homogeneous ORR reaction.[138-141]

In this perspective we have discussed the homogeneous ORR activity of the known Mn-based systems in comparison to comparable Fe and Co analogues. Based only on a limited number of examples, it is clear that mechanistic understanding can allow for the successful development of new Mn-based catalysts through non-covalent effects, choice of redox mediators, or use of dinuclear active species. Possible future, but unproven, strategies for ORR catalysis with Mn active sites could include judicious choice of axial ligand (possibly in control with equatorial ligand manipulation). Mechanistic studies by the groups of Kovacs and Jackson have demonstrated how the manipulation of the electronic properties and steric profiles of ligand frameworks can impart control over Mn-O_2 adducts, which could also be leveraged into catalytic systems.[73, 142] Likewise, it is also possible that intrinsic factors which make Mn compounds excel at the disproportionation of superoxide and activation of hydrogen peroxide could be translated to the ORR.[143-148]

In spite of the successes known from the effect of analogous modifications on Fe- and Co-based catalysts, development of comparable examples with Mn has lagged behind. For Mn, we speculate that its low activity results from its preference for open-shell

configurations, which can facilitate the activation of O_2 beyond superoxide and the formation of intrinsically stable side-on modes, limiting kinetics. However, we are optimistic that the known successes in this area, coupled with the analysis presented here, can prove useful to researchers interested in expanding the number of known Mn-based catalysts for homogeneous ORR.

Author Contributions

The manuscript was written through the contribution of all authors.

Funding Sources

We thank the University of Virginia for infrastructural support as well as N.S.F. CHE-2102156 and ACS PRF 61430-ND3 for financial support.

References

1. Kovaleva, E. G.; Lipscomb, J. D. Versatility of biological non-heme Fe(II) centers in oxygen activation reactions. *Nat. Chem. Biol.* **2008,** 4 (3), 186-193 DOI: 10.1038/nchembio.71.
2. Blomberg, M. R. A. Mechanism of Oxygen Reduction in Cytochrome c Oxidase and the Role of the Active Site Tyrosine. *Biochemistry* **2016,** 55 (3), 489-500 DOI: 10.1021/acs.biochem.5b01205.
3. Denisov, I. G.; Makris, T. M.; Sligar, S. G.; Schlichting, I. Structure and Chemistry of Cytochrome P450. *Chem. Rev.* **2005,** 105 (6), 2253-2278 DOI: 10.1021/cr0307143.
4. Pegis, M. L.; Wise, C. F.; Martin, D. J.; Mayer, J. M. Oxygen Reduction by Homogeneous Molecular Catalysts and Electrocatalysts. *Chem. Rev.* **2018,** 118 (5), 2340-2391 DOI: 10.1021/acs.chemrev.7b00542.
5. Yoshikawa, S.; Shimada, A. Reaction mechanism of cytochrome c oxidase. *Chemical Reviews* **2015,** 115 (4), 1936-1989 DOI: 10.1021/cr500266a.
6. Campbell, A. N.; Stahl, S. S. Overcoming the "Oxidant Problem": Strategies to Use O2 as the Oxidant in Organometallic C–H Oxidation Reactions Catalyzed by Pd (and Cu). *Acc. Chem. Res.* **2012,** 45 (6), 851-863 DOI: 10.1021/ar2002045.
7. Kiani, M.; Tian, X. Q.; Zhang, W. Non-precious metal electrocatalysts design for oxygen reduction reaction in polymer electrolyte membrane fuel cells: Recent advances, challenges and future perspectives. *Coordination Chemistry Reviews* **2021,** 441, 213954 DOI: https://doi.org/10.1016/j.ccr.2021.213954.
8. Wang, Y.; Waterhouse, G. I. N.; Shang, L.; Zhang, T. Electrocatalytic Oxygen Reduction to Hydrogen Peroxide: From Homogeneous to Heterogeneous Electrocatalysis. *Adv. Energ. Mat.* **2021,** 11 (15), 2003323 DOI: https://doi.org/10.1002/aenm.202003323.
9. Campos-Martin, J. M.; Blanco-Brieva, G.; Fierro, J. L. G. Hydrogen peroxide synthesis: An outlook beyond the anthraquinone process. *Angew. Chem., Int. Ed.* **2006,** 45 (42), 6962-6984 DOI: 10.1002/anie.200503779.
10. Fukuzumi, S.; Yamada, Y.; Karlin, K. D. Hydrogen peroxide as a sustainable energy carrier: Electrocatalytic production of hydrogen peroxide and the fuel cell. *Electrochim. Acta* **2012,** 82, 493-511 DOI: https://doi.org/10.1016/j.electacta.2012.03.132.
11. Saouma, C. T.; Mayer, J. M. Do spin state and spin density affect hydrogen atom transfer reactivity? *Chem. Sci.* **2014,** 5 (1), 21-31 DOI: 10.1039/C3SC52664J.
12. Solomon, E. I.; Goudarzi, S.; Sutherlin, K. D. O2 Activation by Non-Heme Iron Enzymes. *Biochemistry* **2016,** 55 (46), 6363-6374 DOI: 10.1021/acs.biochem.6b00635.
13. Rittle, J.; Green, M. T. Cytochrome P450 Compound I: Capture, Ch. *Science* **2010,** 330 (6006), 933-937 DOI: 10.1126/science.1193478.
14. Andreou, A.; Feussner, I. Lipoxygenases - Structure and reaction mechanism. *Phytochemistry* **2009,** 70 (13-14), 1504-1510 DOI: 10.1016/j.phytochem.2009.05.008.
15. Sheng, Y.; Abreu, I. A.; Cabelli, D. E.; Maroney, M. J.; Miller, A. F.; Teixeira, M.; Valentine, J. S. Superoxide dismutases and superoxide reductases. *Chem. Rev.* **2014,** 114 (7), 3854-3918 DOI: 10.1021/cr4005296.

16. Costas, M.; Mehn, M. P.; Jensen, M. P.; Que, L. Dioxygen Activation at Mononuclear Nonheme Iron Active Sites: Enzymes, Models, and Intermediates. *Chemical Reviews* **2004,** 104 (2), 939-986 DOI: 10.1021/cr020628n.
17. Decker, A.; Solomon, E. I. Dioxygen activation by copper, heme and non-heme iron enzymes: Comparison of electronic structures and reactivities. *Curr. Opin. Chem. Biol.* **2005,** 9 (2), 152-163 DOI: 10.1016/j.cbpa.2005.02.012.
18. Kovaleva, E. G.; Neibergall, M. B. Finding Intermediates in the O 2 Activation Pathways of Non-Heme Iron Oxygenases. **2007**, 475-483.
19. Yano, J.; Yachandra, V. Mn4Ca Cluster in Photosynthesis: Where and How Water is Oxidized to Dioxygen. *Chem. Rev.* **2014,** 114 (8), 4175-4205 DOI: 10.1021/cr4004874.
20. Umena, Y.; Kawakami, K.; Shen, J.-R.; Kamiya, N. Crystal structure of oxygen-evolving photosystem II at a resolution of 1.9 Å. *Nature* **2011,** 473 (7345), 55-60 DOI: 10.1038/nature09913.
21. Zhang, W.; Lai, W.; Cao, R. Energy-Related Small Molecule Activation Reactions: Oxygen Reduction and Hydrogen and Oxygen Evolution Reactions Catalyzed by Porphyrin- and Corrole-Based Systems. *Chem. Rev.* **2017,** 117 (4), 3717-3797 DOI: 10.1021/acs.chemrev.6b00299.
22. Li, X.; Lei, H.; Xie, L.; Wang, N.; Zhang, W.; Cao, R. Metalloporphyrins as Catalytic Models for Studying Hydrogen and Oxygen Evolution and Oxygen Reduction Reactions. *Acc. Chem. Res.* **2022,** 55 (6), 878-892 DOI: 10.1021/acs.accounts.1c00753.
23. Paul, S.; Neese, F.; Pantazis, D. A. Structural models of the biological oxygen-evolving complex: achievements, insights, and challenges for biomimicry. *Green Chem.* **2017,** 19 (10), 2309-2325 DOI: 10.1039/C7GC00425G.
24. Cook, E. N.; Machan, C. W. Bioinspired mononuclear Mn complexes for O2 activation and biologically relevant reactions. *Dalton Trans.* **2021,** 50 (46), 16871-16886 DOI: 10.1039/D1DT03178C.
25. Machan, C. W. Advances in the Molecular Catalysis of Dioxygen Reduction. *ACS Catal.* **2020,** 10 (4), 2640-2655 DOI: 10.1021/acscatal.9b04477.
26. Langerman, M.; Hetterscheid, D. G. H. Fast Oxygen Reduction Catalyzed by a Copper(II) Tris(2-pyridylmethyl)amine Complex through a Stepwise Mechanism. *Angew. Chem., Int. Ed.* **2019,** 58 (37), 12974-12978 DOI: 10.1002/anie.201904075.
27. Gewirth, A. A.; Varnell, J. A.; DiAscro, A. M. Nonprecious Metal Catalysts for Oxygen Reduction in Heterogeneous Aqueous Systems. *Chem. Rev.* **2018,** 118 (5), 2313-2339 DOI: 10.1021/acs.chemrev.7b00335.
28. Shao, M.; Chang, Q.; Dodelet, J. P.; Chenitz, R. Recent Advances in Electrocatalysts for Oxygen Reduction Reaction. *Chem. Rev.* **2016,** 116 (6), 3594-3657 DOI: 10.1021/acs.chemrev.5b00462.
29. Wang, X.; Li, Z.; Qu, Y.; Yuan, T.; Wang, W.; Wu, Y.; Li, Y. Review of Metal Catalysts for Oxygen Reduction Reaction: From Nanoscale Engineering to Atomic Design. *Chem* **2019,** 5 (6), 1486-1511 DOI: https://doi.org/10.1016/j.chempr.2019.03.002.
30. Li, J.; Chen, M.; Cullen, D. A.; Hwang, S.; Wang, M.; Li, B.; Liu, K.; Karakalos, S.; Lucero, M.; Zhang, H.; Lei, C.; Xu, H.; Sterbinsky, G. E.; Feng, Z.; Su, D.; More,

K. L.; Wang, G.; Wang, Z.; Wu, G. Atomically dispersed manganese catalysts for oxygen reduction in proton-exchange membrane fuel cells. *Nat. Catal.* **2018,** 1 (12), 935-945 DOI: 10.1038/s41929-018-0164-8.

31. Liu, D. D.; Tao, L.; Yan, D. F.; Zou, Y. Q.; Wang, S. Y. Recent advances on non-precious metal porous carbon-based electrocatalysts for oxygen reduction reaction. *ChemElectroChem* **2018,** 5, 1775-1785 DOI: 10.1002/celc.201800086.
32. Yang, Y.; Mao, K.; Gao, S.; Huang, H.; Xia, G.; Lin, Z.; Jiang, P.; Wang, C.; Wang, H.; Chen, Q. O-, N-Atoms-Coordinated Mn Cofactors within a Graphene Framework as Bioinspired Oxygen Reduction Reaction Electrocatalysts. *Adv. Mat.* **2018,** 30 (28), 1801732 DOI: https://doi.org/10.1002/adma.201801732.
33. Huang, X.; Shen, T.; Zhang, T.; Qiu, H.; Gu, X.; Ali, Z.; Hou, Y. Efficient Oxygen Reduction Catalysts of Porous Carbon Nanostructures Decorated with Transition Metal Species. *Adv. Energ. Mat.* **2020,** 10 (11), 1900375 DOI: https://doi.org/10.1002/aenm.201900375.
34. Lai, Q. X.; Zheng, J.; Tang, Z. M.; Bi, D.; Zhao, J. X.; Liang, Y. Y. Optimal configuration of N-doped carbon defects in 2D turbostratic carbon nanomesh for advanced oxygen reduction electrocatalysis. *Angew. Chem., Int. Ed.* **2020,** 59, 11999-12006 DOI: 10.1002/anie.202000936.
35. Lin, Z.; Huang, H.; Cheng, L.; Yang, Y.; Zhang, R.; Chen, Q. Atomically Dispersed Mn within Carbon Frameworks as High-Performance Oxygen Reduction Electrocatalysts for Zinc–Air Battery. *ACS Sus. Chem. Eng.* **2020,** 8 (1), 427-434 DOI: 10.1021/acssuschemeng.9b05713.
36. Wang, Y.; Zhang, X.; Xi, S.; Xiang, X.; Du, Y.; Chen, P.; Lyu, D.; Wang, S.; Tian, Z. Q.; Shen, P. K. Rational Design and Synthesis of Hierarchical Porous Mn–N–C Nanoparticles with Atomically Dispersed MnNx Moieties for Highly Efficient Oxygen Reduction Reaction. *ACS Sus. Chem. Eng.* **2020,** 8 (25), 9367-9376 DOI: 10.1021/acssuschemeng.0c01882.
37. Wan, C.; Duan, X.; Huang, Y. Molecular Design of Single-Atom Catalysts for Oxygen Reduction Reaction. *Adv. Energ. Mat.* **2020,** 10 (14), 1903815 DOI: https://doi.org/10.1002/aenm.201903815.
38. Li, L.; Li, Y.; Huang, R.; Cao, X.; Wen, Y. Single Mn Atom Anchored on Nitrogen-Doped Graphene as a Highly Efficient Electrocatalyst for Oxygen Reduction Reaction. *Chem. – Eur. J.* **2021,** 27 (37), 9686-9693 DOI: https://doi.org/10.1002/chem.202101020.
39. Tian, P.; Zang, J.; Dong, L.; Song, S.; Zhou, S.; Gao, H.; Tian, X.; Wang, Y. Manganese coordinated with nitrogen in aligned hierarchical porous carbon for efficient electrocatalytic oxygen reduction reaction in alkaline and acidic medium. *Int. J. Hyd. Energ.* **2021,** 46 (1), 543-554 DOI: https://doi.org/10.1016/j.ijhydene.2020.09.230.
40. Zhao, C.-X.; Li, B.-Q.; Liu, J.-N.; Zhang, Q. Intrinsic Electrocatalytic Activity Regulation of M–N–C Single-Atom Catalysts for the Oxygen Reduction Reaction. *Angew. Chem., Int. Ed.* **2021,** 60 (9), 4448-4463 DOI: https://doi.org/10.1002/anie.202003917.
41. Chao, G.; Zhang, Y.; Zhang, L.; Zong, W.; Zhang, N.; Xue, T.; Fan, W.; Liu, T.; Xie, Y. Nitrogen-coordinated single-atom catalysts with manganese and cobalt sites for

acidic oxygen reduction. *J. Mat. Chem. A* **2022,** 10 (11), 5930-5936 DOI: 10.1039/D1TA08029F.

42. Deng, Y.; Pang, J.; Ge, W.; Zhang, M.; Zhang, W.; Zhang, W.; Xiang, M.; Zhou, Q.; Bai, J. Constructing atomically-dispersed Mn on ZIF-derived nitrogen-doped carbon for boosting oxygen reduction. *Front. Chem.* **2022,** 10.
43. Kong, Z.; Wang, H.; Hou, K.; Guan, L. High-performance manganese and nitrogen codoped carbon (Mn–N–C) oxygen reduction electrocatalyst from Mn²⁺ coordinated sodium alginate. *Nanotechnology* **2022,** 33 (24), 245701 DOI: 10.1088/1361-6528/ac5aed.
44. Hamilton, G. A.; Revesz, A. Oxidation by Molecular Oxygen. IV. A Possible Model Reaction for Some Amine Oxidases1-3. *J. Am. Chem. Soc.* **1966,** 88 (9), 2069-2070 DOI: 10.1021/ja00961a054.
45. Mondovì, B.; Agrò, A. F. In *Structure and Function Relationships in Biochemical Systems*; Bossa, F., Chiancone, E., Finazzi-Agrò, A., Strom, R., Ed.; Springer US: Boston, MA, 1982; pp 141-153.
46. Davies, G. Some aspects of the chemistry of manganese(III) in aqueous solution. *Coord. Chem. Rev.* **1969,** 4 (2), 199-224 DOI: https://doi.org/10.1016/S0010-8545(00)80086-7.
47. Bettelheim, A.; Ozer, D.; Parash, R. Electrochemical and spectroscopic properties of manganese tetra(4-NN′N″-trimethylanilinium)porphyrin. *J. Chem. Soc., Faraday Trans. 1: Phys. Chem. Cond. Phases* **1983,** 79 (7), 1555-1564 DOI: 10.1039/F19837901555.
48. Nagao, K.; Hiroshi, S.; Tetsuo, O. Catalytic Electroreduction of Molecular Oxygen Using [5,10,15,20-tetrakis-(1-methylpyridinium-4-yl)porphinato]manganese. *Chem. Lett.* **1985,** 14 (12), 1917-1920 DOI: 10.1246/cl.1985.1917.
49. Costentin, C.; Dridi, H.; Savéant, J.-M. Molecular Catalysis of O2 Reduction by Iron Porphyrins in Water: Heterogeneous versus Homogeneous Pathways. *J. Am. Chem. Soc.* **2015,** 137 (42), 13535-13544 DOI: 10.1021/jacs.5b06834.
50. Evans, D. F.; Sheriff, T. S. The production of hydrogen peroxide from dioxygen and hydroxylamine catalysed by manganese complexes. *J. Chem. Soc., Chem. Commun.* **1985,** (20), 1407-1408 DOI: 10.1039/C39850001407.
51. Sheriff, T. S. Production of hydrogen peroxide from dioxygen and hydroxylamine or hydrazine catalysed by manganese complexes. *J. Chem. Soc., Dalton Trans.* **1992,** (6), 1051-1058 DOI: 10.1039/DT9920001051.
52. Fukuzumi, S.; Mochizuki, S.; Tanaka, T. Metalloporphyrin-Catalyzed Reduction of Dioxygen by Ferrocene Derivatives. *Chem. Lett.* **1989,** 18 (1), 27-30 DOI: 10.1246/cl.1989.27.
53. Fukuzumi, S.; Mochizuki, S.; Tanaka, T. Efficient reduction of dioxygen with ferrocene derivatives, catalyzed by metalloporphyrins in the presence of perchloric acid. *Inorg. Chem.* **1989,** 28 (12), 2459-2465 DOI: 10.1021/ic00311a042.
54. Noviandri, I.; Brown, K. N.; Fleming, D. S.; Gulyas, P. T.; Lay, P. A.; Masters, A. F.; Phillips, L. The Decamethylferrocenium/Decamethylferrocene Redox Couple: A Superior Redox Standard to the Ferrocenium/Ferrocene Redox Couple for Studying Solvent Effects on the Thermodynamics of Electron Transfer. *J. Phys. Chem. B* **1999,** 103 (32), 6713-6722 DOI: 10.1021/jp991381+.

55. Shook, R. L.; Peterson, S. M.; Greaves, J.; Moore, C.; Rheingold, A. L.; Borovik, A. S. Catalytic Reduction of Dioxygen to Water with a Monomeric Manganese Complex at Room Temperature. *J. Am. Chem. Soc.* **2011,** 133 (15), 5810-5817 DOI: 10.1021/ja106564a.
56. Costentin, C.; Drouet, S.; Robert, M.; Savéant, J.-M. A Local Proton Source Enhances CO2 Electroreduction to CO by a Molecular Fe Catalyst. *Science* **2012,** 338 (6103), 90–94 DOI: 10.1126/science.1224581.
57. Azcarate, I.; Costentin, C.; Robert, M.; Savéant, J.-M. Through-Space Charge Interaction Substituent Effects in Molecular Catalysis Leading to the Design of the Most Efficient Catalyst of CO2-to-CO Electrochemical Conversion. *J. Am. Chem. Soc.* **2016,** 138 (51), 16639-16644 DOI: 10.1021/jacs.6b07014.
58. Nichols, A. W.; Machan, C. W. Secondary-Sphere Effects in Molecular Electrocatalytic CO2 Reduction. *Front. Chem.* **2019,** 7, https://doi.org/10.3389/fchem.2019.00397.
59. Nichols, A. W.; Cook, E. N.; Gan, Y. J.; Miedaner, P. R.; Dressel, J. M.; Dickie, D. A.; Shafaat, H. S.; Machan, C. W. Pendent Relay Enhances H2O2 Selectivity during Dioxygen Reduction Mediated by Bipyridine-Based Co–N2O2 Complexes. *J. Am. Chem. Soc.* **2021,** 143 (33), 13065-13073 DOI: 10.1021/jacs.1c03381.
60. Nichols, Eva M.; Derrick, J. S.; Nistanaki, S. K.; Smith, P. T.; Chang, C. J. Positional effects of second-sphere amide pendants on electrochemical CO2 reduction catalyzed by iron porphyrins. *Chem. Sci.* **2018,** 9 (11), 2952-2960 DOI: 10.1039/C7SC04682K.
61. Gotico, P.; Boitrel, B.; Guillot, R.; Sircoglou, M.; Quaranta, A.; Halime, Z.; Leibl, W.; Aukauloo, A. Second-Sphere Biomimetic Multipoint Hydrogen-Bonding Patterns to Boost CO2 Reduction of Iron Porphyrins. *Angew. Chem., Int. Ed.* **2019,** 58 (14), 4504-4509 DOI: https://doi.org/10.1002/anie.201814339.
62. Gotico, P.; Roupnel, L.; Guillot, R.; Sircoglou, M.; Leibl, W.; Halime, Z.; Aukauloo, A. Atropisomeric Hydrogen Bonding Control for CO2 Binding and Enhancement of Electrocatalytic Reduction at Iron Porphyrins. *Angew. Chem., Int. Ed.* **2020,** 59 (50), 22451-22455 DOI: https://doi.org/10.1002/anie.202010859.
63. Rakowski Dubois, M.; Dubois, D. L. Development of Molecular Electrocatalysts for CO2 Reduction and H2 Production/Oxidation. *Acc. Chem. Res.* **2009,** 42 (12), 1974-1982 DOI: 10.1021/ar900110c.
64. DuBois, D. L. Development of Molecular Electrocatalysts for Energy Storage. *Inorganic Chemistry* **2014,** 53 (8), 3935-3960 DOI: 10.1021/ic4026969.
65. Shaw, W. J. The Outer-Coordination Sphere: Incorporating Amino Acids and Peptides as Ligands for Homogeneous Catalysts to Mimic Enzyme Function. *Catal. Rev.* **2012,** 54 (4), 489-550 DOI: 10.1080/01614940.2012.679453.
66. He, Q.; Mugadza, T.; Hwang, G.; Nyokong, T. Mechanisms of Electrocatalysis of Oxygen Reduction by Metal Porphyrins in Trifluoromethane Sulfonic Acid Solution *Int. J. Electrochem. Sci.* **2012,** 7 (8), 7045 - 7064.
67. Trummal, A.; Lipping, L.; Kaljurand, I.; Koppel, I. A.; Leito, I. Acidity of Strong Acids in Water and Dimethyl Sulfoxide. *J. Phys. Chem. A* **2016,** 120 (20), 3663-3669 DOI: 10.1021/acs.jpca.6b02253.

68. Lieske, L. E.; Hooe, S. L.; Nichols, A. W.; Machan, C. W. Electrocatalytic reduction of dioxygen by Mn(iii) meso-tetra(N-methylpyridinium-4-yl)porphyrin in universal buffer. *Dalton Trans.* **2019,** 48, 8633-8641 DOI: 10.1039/C9DT01436E.
69. Winkler, J. R.; Gray, H. B. In *Molecular Electronic Structures of Transition Metal Complexes I*; Mingos, D. M. P., Day, P., Dahl, J. P., Ed.; Springer: Heidelberg Dordrecht London New York, 2011; Vol. 142, pp 17-28.
70. Gennari, M.; Brazzolotto, D.; Pécaut, J.; Cherrier, M. V.; Pollock, C. J.; Debeer, S.; Retegan, M.; Pantazis, D. A.; Neese, F.; Rouzières, M.; Clérac, R.; Duboc, C. Dioxygen Activation and Catalytic Reduction to Hydrogen Peroxide by a Thiolate-Bridged Dimanganese(II) Complex with a Pendant Thiol. *J. Am. Chem. Soc.* **2015,** 137 (26), 8644-8653 DOI: 10.1021/jacs.5b04917.
71. Coggins, M. K.; Toledo, S.; Shaffer, E.; Kaminsky, W.; Shearer, J.; Kovacs, J. A. Characterization and dioxygen reactivity of a new series of coordinatively unsaturated thiolate-ligated manganese(II) complexes. *Inorg. Chem.* **2012,** 51 (12), 6633-6644 DOI: 10.1021/ic300192q.
72. Coggins, M. K.; Sun, X.; Kwak, Y.; Solomon, E. I.; Rybak-Akimova, E.; Kovacs, J. A. Characterization of Metastable Intermediates Formed in the Reaction between a Mn(II) Complex and Dioxygen, Including a Crystallographic Structure of a Binuclear Mn(III)–Peroxo Species. *J. Am. Chem. Soc.* **2013,** 135 (15), 5631-5640 DOI: 10.1021/ja311166u.
73. Kovacs, J. A. Tuning the Relative Stability and Reactivity of Manganese Dioxygen and Peroxo Intermediates via Systematic Ligand Modification. *Acc. Chem. Res.* **2015,** 48 (10), 2744-2753 DOI: 10.1021/acs.accounts.5b00260.
74. Chaau Yan Poon, P.; Dedushko, M. A.; Sun, X.; Yang, G.; Toledo, S.; Hayes, E. C.; Johansen, A.; Piquette, M. C.; Rees, J. A.; Stoll, S.; Rybak-akimova, E.; Kovacs, J. A. How Metal Ion Lewis Acidity and Steric Properties Influence the Barrier to Dioxygen Binding, Peroxo O-O Bond Cleavage, and Reactivity. *J. Am. Chem. Soc.* **2019,** 141, 15046-15057 DOI: 10.1021/jacs.9b04729.
75. Downing, A. N.; Coggins, M. K.; Poon, P. C. Y.; Kovacs, J. A. Influence of Thiolate versus Alkoxide Ligands on the Stability of Crystallographically Characterized Mn(III)-Alkylperoxo Complexes. *J. Am. Chem. Soc.* **2021,** 143 (16), 6104-6113 DOI: 10.1021/jacs.0c13001.
76. Wang, L.; Gennari, M.; Cantú Reinhard, F. G.; Gutiérrez, J.; Morozan, A.; Philouze, C.; Demeshko, S.; Artero, V.; Meyer, F.; de Visser, S. P.; Duboc, C. A Non-Heme Diiron Complex for (Electro)catalytic Reduction of Dioxygen: Tuning the Selectivity through Electron Delivery. *J. Am. Chem. Soc.* **2019,** 141 (20), 8244-8253 DOI: 10.1021/jacs.9b02011.
77. Hanson, J. Synthesis and Use of Jacobsen's Catalyst: Enantioselective Epoxidation in the Introductory Organic Laboratory. *J. Chem. Ed.* **2001,** 78 (9), 1266 DOI: 10.1021/ed078p1266.
78. Cozzi, P. G. Metal-Salen Schiff base complexes in catalysis: practical aspects. *Chem. Soc. Rev.* **2004,** 33 (7), 410-421 DOI: 10.1039/B307853C.
79. Machan, C. W.; Chabolla, S. A.; Kubiak, C. P. Reductive Disproportionation of Carbon Dioxide by an Alkyl-Functionalized Pyridine Monoimine Re(I) fac-Tricarbonyl Electrocatalyst. *Organometallics* **2015,** 34 (19), 4678–4683 DOI: 10.1021/acs.organomet.5b00406.

80. Arora, H.; Philouze, C.; Jarjayes, O.; Thomas, F. CoII, NiII, CuII and ZnII complexes of a bipyridine bis-phenol conjugate: Generation and properties of coordinated radical species. *Dalton Trans.* **2010,** 39 (42), 10088–10098 DOI: 10.1039/C0DT00342E.
81. Hooe, S. L.; Rheingold, A. L.; Machan, C. W. Electrocatalytic Reduction of Dioxygen to Hydrogen Peroxide by a Molecular Manganese Complex with a Bipyridine-Containing Schiff Base Ligand. *J. Am. Chem. Soc.* **2018,** 140 (9), 3232-3241 DOI: 10.1021/jacs.7b09027.
82. McCarthy, B. D.; Dempsey, J. L. Decoding Proton-Coupled Electron Transfer with Potential-pKa Diagrams. *Inorg. Chem.* **2017,** 56 (3), 1225-1231 DOI: 10.1021/acs.inorgchem.6b02325.
83. Hooe, S. L.; Machan, C. W. Dioxygen Reduction to Hydrogen Peroxide by a Molecular Mn Complex: Mechanistic Divergence between Homogeneous and Heterogeneous Reductants. *J. Am. Chem. Soc.* **2019,** 141 (10), 4379-4387 DOI: 10.1021/jacs.8b13373.
84. Pegis, M. L.; Roberts, J. A. S.; Wasylenko, D. J.; Mader, E. A.; Appel, A. M.; Mayer, J. M. Standard Reduction Potentials for Oxygen and Carbon Dioxide Couples in Acetonitrile and N,N-Dimethylformamide. *Inorg. Chem.* **2015,** 54 (24), 11883-11888 DOI: 10.1021/acs.inorgchem.5b02136.
85. Passard, G.; Dogutan, D. K.; Qiu, M.; Costentin, C.; Nocera, D. G. Oxygen Reduction Reaction Promoted by Manganese Porphyrins. *ACS Catal.* **2018,** 8 (9), 8671-8679 DOI: 10.1021/acscatal.8b01944.
86. Weitner, T.; Budimir, A.; Kos, I.; Batinić-Haberle, I.; Biruš, M. Acid–base and electrochemical properties of manganese meso(ortho- and meta-N-ethylpyridyl)porphyrins: potentiometric, spectrophotometric and spectroelectrochemical study of protolytic and redox equilibria. *Dalton Trans.* **2010,** 39 (48), 11568-11576 DOI: 10.1039/C0DT00585A.
87. Weitner, T.; Kos, I.; Mandić, Z.; Batinić-Haberle, I.; Biruš, M. Acid–base and electrochemical properties of manganese meso(ortho- and meta-N-ethylpyridyl)porphyrins: voltammetric and chronocoulometric study of protolytic and redox equilibria. *Dalton Trans.* **2013,** 42 (41), 14757-14765 DOI: 10.1039/C3DT50767J.
88. Naruta, Y.; Sasayama, M.-A. Importance of Mn–Mn separation and their relative arrangement on the development of high catalase activity in manganese porphyrin dimer catalysts. *J. Chem. Soc., Chem. Comm.* **1994,** (23), 2667-2668 DOI: 10.1039/C39940002667.
89. Balasubramanian, P. N.; Schmidt, E. S.; Bruice, T. C. Catalase modeling. 2. Dynamics of reaction of a water-soluble and non .mu.-oxo dimer forming manganese(III) porphyrin with hydrogen peroxide. *J. Am. Chem. Soc.* **1987,** 109 (25), 7865-7873 DOI: 10.1021/ja00259a040.
90. Carnieri, N.; Harriman, A.; Porter, G. Photochemistry of manganese porphyrins. Part 6. Oxidation–reduction equilibria of manganese(III) porphyrins in aqueous solution. *J. Chem. Soc., Dalton Trans.* **1982,** (5), 931-938 DOI: 10.1039/DT9820000931.
91. Harriman, A. Photochemistry of manganese porphyrins. Part 8. Electrochemistry. *J. Chem. Soc., Dalton Trans.* **1984,** (2), 141-146 DOI: 10.1039/DT9840000141.

92. Harriman, A.; Porter, G. Photochemistry of manganese porphyrins. Part 1.—Characterisation of some water soluble complexes. *J. Chem. Soc., Faraday Trans. 2* **1979,** 75 (0), 1532-1542 DOI: 10.1039/F29797501532.
93. Hooe, S. L.; Cook, E. N.; Reid, A. G.; Machan, C. W. Non-covalent assembly of proton donors and p- benzoquinone anions for co-electrocatalytic reduction of dioxygen. *Chem. Sci.* **2021,** 12 (28), 9733-9741 DOI: 10.1039/d1sc01271a.
94. Anson, C. W.; Stahl, S. S. Cooperative Electrocatalytic O2 Reduction Involving Co(salophen) with p-Hydroquinone as an Electron–Proton Transfer Mediator. *J. Am. Chem. Soc.* **2017,** 139 (51), 18472-18475 DOI: 10.1021/jacs.7b11362.
95. Anson, C. W.; Ghosh, S.; Hammes-Schiffer, S.; Stahl, S. S. Co(salophen)-Catalyzed Aerobic Oxidation of p-Hydroquinone: Mechanism and Implications for Aerobic Oxidation Catalysis. *J. Am. Chem. Soc.* **2016,** 138 (12), 4186-4193 DOI: 10.1021/jacs.6b00254.
96. Huynh, M. T.; Anson, C. W.; Cavell, A. C.; Stahl, S. S.; Hammes-Schiffer, S. Quinone 1 e– and 2 e–/2 H+ Reduction Potentials: Identification and Analysis of Deviations from Systematic Scaling Relationships. *J. Am. Chem. Soc.* **2016,** 138 (49), 15903-15910 DOI: 10.1021/jacs.6b05797.
97. Gupta, N.; Linschitz, H. Hydrogen-Bonding and Protonation Effects in Electrochemistry of Quinones in Aprotic Solvents. *J. Am. Chem. Soc.* **1997,** 119 (27), 6384-6391 DOI: 10.1021/ja970028j.
98. Costentin, C. Electrochemical Approach to the Mechanistic Study of Proton-Coupled Electron Transfer. *Chem. Rev.* **2008,** 108 (7), 2145-2179 DOI: 10.1021/cr068065t.
99. Quan, M.; Sanchez, D.; Wasylkiw, M. F.; Smith, D. K. Voltammetry of Quinones in Unbuffered Aqueous Solution: Reassessing the Roles of Proton Transfer and Hydrogen Bonding in the Aqueous Electrochemistry of Quinones. *J. Am. Chem. Soc.* **2007,** 129 (42), 12847-12856 DOI: 10.1021/ja0743083.
100. Staley, P. A.; Lopez, E. M.; Clare, L. A.; Smith, D. K. Kinetic Stabilization of Quinone Dianions via Hydrogen Bonding by Water in Aprotic Solvents. *J. Phys. Chem. C* **2015,** 119 (35), 20319-20327 DOI: 10.1021/acs.jpcc.5b06323.
101. Evans, D. H. One-Electron and Two-Electron Transfers in Electrochemistry and Homogeneous Solution Reactions. *Chem. Rev.* **2008,** 108 (7), 2113-2144 DOI: 10.1021/cr068066l.
102. Astudillo, P. D.; Tiburcio, J.; González, F. J. The role of acids and bases on the electrochemical oxidation of hydroquinone: Hydrogen bonding interactions in acetonitrile. *J. Electroanal. Chem.* **2007,** 604 (1), 57-64 DOI: https://doi.org/10.1016/j.jelechem.2007.02.031.
103. Astudillo, P. D.; Valencia, D. P.; González-Fuentes, M. A.; Díaz-Sánchez, B. R.; Frontana, C.; González, F. J. Electrochemical and chemical formation of a low-barrier proton transfer complex between the quinone dianion and hydroquinone. *Electrochim. Acta* **2012,** 81, 197-204 DOI: https://doi.org/10.1016/j.electacta.2012.07.078.
104. Alligrant, T. M.; Hackett, J. C.; Alvarez, J. C. Acid/base and hydrogen bonding effects on the proton-coupled electron transfer of quinones and hydroquinones in acetonitrile: Mechanistic investigation by voltammetry, 1H NMR and computation.

Electrochim. Acta **2010,** 55 (22), 6507-6516 DOI: https://doi.org/10.1016/j.electacta.2010.06.029.

105. Lam, Y. C.; Nielsen, R. J.; Gray, H. B.; Goddard, W. A. A Mn Bipyrimidine Catalyst Predicted To Reduce CO2 at Lower Overpotential. *ACS Catal.* **2015,** 5 (4), 2521-2528 DOI: 10.1021/cs501963v.
106. Macías-Ruvalcaba, N. A.; Okumura, N.; Evans, D. H. Change in Reaction Pathway in the Reduction of 3,5-Di-tert-butyl-1,2-benzoquinone with Increasing Concentrations of 2,2,2-Trifluoroethanol. *J. Phys. Chem. B* **2006,** 110 (43), 22043-22047 DOI: 10.1021/jp064003v.
107. Evans, D. H.; René, A. Reinvestigation of a former concerted proton-electron transfer (CPET), the reduction of a hydrogen-bonded complex between a proton donor and the anion radical of 3,5-di-tert-butyl-1,2-benzoquinone. *Phys. Chem. Chem. Phys.* **2012,** 14 (14), 4844-4848 DOI: 10.1039/C2CP00021K.
108. Niederhoffer, E. C.; Timmons, J. H.; Martell, A. E. Thermodynamics of oxygen binding in natural and synthetic dioxygen complexes. *Chem. Rev.* **1984,** 84 (2), 137-203 DOI: 10.1021/cr00060a003.
109. Degtyarenko, I.; Nieminen, R. M.; Rovira, C. Structure and Dynamics of Dioxygen Bound to Cobalt and Iron Heme. *Biophysical Journal* **2006,** 91 (6), 2024-2034 DOI: 10.1529/biophysj.106.083048.
110. Zaragoza, J. P. T.; Goldberg, D. P. In *Dioxygen-dependent Heme Enzymes*; The Royal Society of Chemistry: 2019; pp 1-36.
111. F. Albert Cotton, G. W., Carlos A. Murillo, Manfred Bochmann. *Advanced Inorganic Chemistry, 6th Edition*. Wiley: 1999; p 1376.
112. Fukuzumi, S.; Lee, Y. M.; Nam, W. Mechanisms of Two-Electron versus Four-Electron Reduction of Dioxygen Catalyzed by Earth-Abundant Metal Complexes. *ChemCatChem* **2018,** 10 (1), 9-28 DOI: 10.1002/cctc.201701064.
113. Zagal, J. H.; Koper, M. T. M. Reactivity Descriptors for the Activity of Molecular MN4 Catalysts for the Oxygen Reduction Reaction. *Angew. Chem., Int. Ed.* **2016,** 55 (47), 14510-14521 DOI: https://doi.org/10.1002/anie.201604311.
114. Sabatier, P. Hydrogénations et déshydrogénations par catalyse. *Chem. Ber.* **1911,** 44 (3), 1984-2001 DOI: https://doi.org/10.1002/cber.19110440303.
115. Costentin, C.; Savéant, J.-M. Homogeneous Molecular Catalysis of Electrochemical Reactions: Manipulating Intrinsic and Operational Factors for Catalyst Improvement. *J. Am. Chem. Soc.* **2018,** 140 (48), 16669-16675 DOI: 10.1021/jacs.8b09154.
116. Pegis, M. L.; McKeown, B. A.; Kumar, N.; Lang, K.; Wasylenko, D. J.; Zhang, X. P.; Raugei, S.; Mayer, J. M. Homogenous electrocatalytic oxygen reduction rates correlate with reaction overpotential in acidic organic solutions. *ACS Cent. Sci.***2016,** 2 (11), 850-856 DOI: 10.1021/acscentsci.6b00261.
117. Flyagina, I. S.; Hughes, K. J.; Pourkashanian, M.; Ingham, D. B. DFT study of the oxygen reduction reaction on iron, cobalt and manganese macrocycle active sites. *Int. J. Hyd. Energ.* **2014,** 39 (36), 21538-21546 DOI: https://doi.org/10.1016/j.ijhydene.2014.09.075.
118. Baran, J. D.; Grönbeck, H.; Hellman, A. Analysis of Porphyrines as Catalysts for Electrochemical Reduction of O2 and Oxidation of H2O. *J. Am. Chem. Soc.* **2014,** 136 (4), 1320-1326 DOI: 10.1021/ja4060299.

119. Chen, H.; Ikeda-Saito, M.; Shaik, S. Nature of the Fe−O2 Bonding in Oxy-Myoglobin: Effect of the Protein. *J. Am. Chem. Soc.* **2008,** 130 (44), 14778-14790 DOI: 10.1021/ja805434m.
120. VanAtta, R. B.; Strouse, C. E.; Hanson, L. K.; Valentine, J. S. Peroxo(tetraphenylporphinato)manganese(III) and chloro(tetraphenylporphinato)manganese(II) anions. Synthesis, crystal structures, and electronic structures. *J. Am. Chem. Soc.* **1987,** 109 (5), 1425-1434 DOI: 10.1021/ja00239a024.
121. Phung, Q. M.; Pierloot, K. The dioxygen adducts of iron and manganese porphyrins: electronic structure and binding energy. *Phys. Chem. Chem. Phys.* **2018,** 20 (25), 17009-17019 DOI: 10.1039/C8CP03078B.
122. Pecoraro, V. L.; Baldwin, M. J.; Gelasco, A. Interaction of Manganese with Dioxygen and Its Reduced Derivatives. *Chem. Rev.* **1994,** 94 (3), 807-826 DOI: 10.1021/cr00027a012.
123. Wang, Y. H.; Schneider, P. E.; Goldsmith, Z. K.; Mondal, B.; Hammes-Schiffer, S.; Stahl, S. S. Brønsted Acid Scaling Relationships Enable Control over Product Selectivity from O2 Reduction with a Mononuclear Cobalt Porphyrin Catalyst. *ACS Cent. Sci.* **2019,** 5 (6), 1024-1034 DOI: 10.1021/acscentsci.9b00194.
124. Collman, J. P.; Yan, Y.-L.; Eberspacher, T.; Xie, X.; Solomon, E. I. Oxygen Binding of Water-Soluble Cobalt Porphyrins in Aqueous Solution. *Inorg. Chem.* **2005,** 44 (26), 9628-9630 DOI: 10.1021/ic0516717.
125. Zhang, R.; Warren, J. J. Controlling the Oxygen Reduction Selectivity of Asymmetric Cobalt Porphyrins by Using Local Electrostatic Interactions. *J. Am. Chem. Soc.* **2020,** 142 (31), 13426-13434 DOI: 10.1021/jacs.0c03861.
126. Walker, F. A. Electron spin resonance study of coordination to the fifth and sixth positions of .alpha.,.beta.,.gamma.,.delta.-tetra(p-methoxyphenyl)porphinatocobalt(II). *J. Am. Chem. Soc.* **1970,** 92 (14), 4235-4244 DOI: 10.1021/ja00717a018.
127. Wasylenko, D. J.; Rodríguez, C.; Pegis, M. L.; Mayer, J. M. Direct Comparison of Electrochemical and Spectrochemical Kinetics for Catalytic Oxygen Reduction. *J. Am. Chem. Soc.* **2014,** 136 (36), 12544-12547 DOI: 10.1021/ja505667t.
128. Pegis, M. L.; Martin, D. J.; Wise, C. F.; Brezny, A. C.; Johnson, S. I.; Johnson, L. E.; Kumar, N.; Raugei, S.; Mayer, J. M. Mechanism of Catalytic O2 Reduction by Iron Tetraphenylporphyrin. *J. Am. Chem. Soc.* **2020,** 141 (20), 8315-8326 DOI: 10.1021/jacs.9b02640.
129. Brezny, A. C.; Johnson, S. I.; Raugei, S.; Mayer, J. M. Selectivity-determining steps in O2 reduction catalyzed by iron(tetramesitylporphyrin). *J. Am. Chem. Soc.* **2020**, DOI: 10.1021/jacs.9b13654.
130. Nichols, A. W.; Kuehner, J. S.; Huffman, B. L.; Miedaner, P. R.; Dickie, D. A.; Machan, C. W. Reduction of dioxygen to water by a Co(N2O2) complex with a 2,2'-bipyridine backbone. *Chem. Commun.* **2021,** 57, 516-519 DOI: 10.1039/d0cc06763f.
131. Wang, Y. H.; Pegis, M. L.; Mayer, J. M.; Stahl, S. S. Molecular Cobalt Catalysts for O2 Reduction: Low-Overpotential Production of H2O2 and Comparison with Iron-Based Catalysts. *J. Am. Chem. Soc.* **2017,** 139 (46), 16458-16461 DOI: 10.1021/jacs.7b09089.

132. Wang, Y.-H.; Goldsmith, Z. K.; Schneider, P. E.; Anson, C. W.; Gerken, J. B.; Ghosh, S.; Hammes-Schiffer, S.; Stahl, S. S. Kinetic and Mechanistic Characterization of Low-Overpotential, H2O2-Selective Reduction of O2 Catalyzed by N2O2-Ligated Cobalt Complexes. *J. Am. Chem. Soc.* **2018,** 140 (34), 10890-10899 DOI: 10.1021/jacs.8b06394.
133. Phung, Q. M.; Wouters, S.; Pierloot, K. Cumulant Approximated Second-Order Perturbation Theory Based on the Density Matrix Renormalization Group for Transition Metal Complexes: A Benchmark Study. *J. Chem. Theo. Comput.* **2016,** 12 (9), 4352-4361 DOI: 10.1021/acs.jctc.6b00714.
134. Waldie, K. M.; Flajslik, K. R.; McLoughlin, E.; Chidsey, C. E. D.; Waymouth, R. M. Electrocatalytic Alcohol Oxidation with Ruthenium Transfer Hydrogenation Catalysts. *J. Am. Chem. Soc.* **2017,** 139 (2), 738-748 DOI: 10.1021/jacs.6b09705.
135. Rafiee, M.; Konz, Z. M.; Graaf, M. D.; Koolman, H. F.; Stahl, S. S. Electrochemical Oxidation of Alcohols and Aldehydes to Carboxylic Acids Catalyzed by 4-Acetamido-TEMPO: An Alternative to “Anelli” and “Pinnick” Oxidations. *ACS Catal.* **2018,** 8 (7), 6738-6744 DOI: 10.1021/acscatal.8b01640.
136. Dey, S.; Masero, F.; Brack, E.; Fontecave, M.; Mougel, V. Electrocatalytic metal hydride generation using CPET mediators. *Nature* **2022,** 607 (7919), 499-506 DOI: 10.1038/s41586-022-04874-z.
137. Reid, A. G.; Moreno, J. J.; Hooe, S. L.; Baugh, K. R.; Thomas, I. H.; Dickie, D. A.; Machan, C. W. Inverse potential scaling in co-electrocatalytic activity for CO2 reduction through redox mediator tuning and catalyst design. *Chem. Sci.* **2022**, DOI: 10.1039/D2SC03258A.
138. Davenport, T. C.; Ahn, H. S.; Ziegler, M. S.; Tilley, T. D. A molecular structural analog of proposed dinuclear active sites in cobalt-based water oxidation catalysts. *Chem. Commun.* **2014,** 50 (48), 6326-6329 DOI: 10.1039/C3CC46865H.
139. Gimbert-Suriñach, C.; Moonshiram, D.; Francàs, L.; Planas, N.; Bernales, V.; Bozoglian, F.; Guda, A.; Mognon, L.; López, I.; Hoque, M. A.; Gagliardi, L.; Cramer, C. J.; Llobet, A. Structural and Spectroscopic Characterization of Reaction Intermediates Involved in a Dinuclear Co–Hbpp Water Oxidation Catalyst. *J. Am. Chem. Soc.* **2016,** 138 (47), 15291-15294 DOI: 10.1021/jacs.6b08532.
140. Rigsby, M. L.; Mandal, S.; Nam, W.; Spencer, L. C.; Llobet, A.; Stahl, S. S. Cobalt analogs of Ru-based water oxidation catalysts: overcoming thermodynamic instability and kinetic lability to achieve electrocatalytic O2 evolution. *Chem. Sci.* **2012,** 3 (10), 3058-3062 DOI: 10.1039/C2SC20755A.
141. Matheu, R.; Garrido-Barros, P.; Gil-Sepulcre, M.; Ertem, M. Z.; Sala, X.; Gimbert-Suriñach, C.; Llobet, A. The development of molecular water oxidation catalysts. *Nat. Rev. Chem.* **2019,** 3 (5), 331-341 DOI: 10.1038/s41570-019-0096-0.
142. Rice, D. B.; Massie, A. A.; Jackson, T. A. Manganese-Oxygen Intermediates in O-O Bond Activation and Hydrogen-Atom Transfer Reactions. *Acc. Chem. Res.* **2017,** 50 (11), 2706-2717 DOI: 10.1021/acs.accounts.7b00343.
143. Miriyala, S.; Spasojevic, I.; Tovmasyan, A.; Salvemini, D.; Vujaskovic, Z.; St Clair, D.; Batinic-Haberle, I. Manganese superoxide dismutase, MnSOD and its mimics. *Biochim Biophys Acta* **2012,** 1822 (5), 794-814 DOI: 10.1016/j.bbadis.2011.12.002.

144. Yu, M.; Ambrose, S. L.; Whaley, Z. L.; Fan, S.; Gorden, J. D.; Beyers, R. J.; Schwartz, D. D.; Goldsmith, C. R. A Mononuclear Manganese(II) Complex Demonstrates a Strategy To Simultaneously Image and Treat Oxidative Stress. *J. Am. Chem. Soc.* **2014,** 136 (37), 12836-12839 DOI: 10.1021/ja507034d.
145. Kenkel, I.; Franke, A.; Dürr, M.; Zahl, A.; Dücker-Benfer, C.; Langer, J.; Filipović, M. R.; Yu, M.; Puchta, R.; Fiedler, S. R.; Shores, M. P.; Goldsmith, C. R.; Ivanović-Burmazović, I. Switching between Inner- and Outer-Sphere PCET Mechanisms of Small-Molecule Activation: Superoxide Dismutation and Oxygen/Superoxide Reduction Reactivity Deriving from the Same Manganese Complex. *J. Am. Chem. Soc.* **2017,** 139 (4), 1472-1484 DOI: 10.1021/jacs.6b08394.
146. Yu, M.; Ward, M. B.; Franke, A.; Ambrose, S. L.; Whaley, Z. L.; Bradford, T. M.; Gorden, J. D.; Beyers, R. J.; Cattley, R. C.; Ivanović-Burmazović, I.; Schwartz, D. D.; Goldsmith, C. R. Adding a Second Quinol to a Redox-Responsive MRI Contrast Agent Improves Its Relaxivity Response to H2O2. *Inorg. Chem.* **2017,** 56 (5), 2812-2826 DOI: 10.1021/acs.inorgchem.6b02964.
147. Friedel, F. C.; Lieb, D.; Ivanović-Burmazović, I. Comparative studies on manganese-based SOD mimetics, including the phosphate effect, by using global spectral analysis. *J. Inorg. Biochem.* **2012,** 109, 26-32 DOI: https://doi.org/10.1016/j.jinorgbio.2011.12.008.
148. Senft, L.; Moore, J. L.; Franke, A.; Fisher, K. R.; Scheitler, A.; Zahl, A.; Puchta, R.; Fehn, D.; Ison, S.; Sader, S.; Ivanović-Burmazović, I.; Goldsmith, C. R. Quinol-containing ligands enable high superoxide dismutase activity by modulating coordination number, charge, oxidation states and stability of manganese complexes throughout redox cycling. *Chem. Sci.* **2021,** 12 (31), 10483-10500 DOI: 10.1039/D1SC02465E.